

Výzkumný úkol:  
PLAZMOVÉ NÁSTŘIKY PRO PERMEAČNÍ BARIÉRY/PLASMA  
SPRAYED PERMEATION BARRIERS  
FJFI ČVUT v Praze  
Katedra fyziky

Bc. Jakub Veverka

## Abstract

Permeační bariéry jsou důležitou součástí materiálového výzkumu pro studium řízené termojaderné fúze. Jejich účelem je zabránit ztrátám izotopů vodíku, zejména tritia, z palivového okruhu budoucích fúzních reaktorů. Toto by mělo za následek únik paliva a radiace z prostoru reaktoru. Praktická realizace spočívá v depozici tenkých vrstev materiálů s nízkou permeabilitou na povrch komponentů množivé obálky a další pomocná vedení, která jsou ohrožená únikem tritia. Mezi tyto materiály patří zejména oxidické keramiky ( $Al_2O_3$ ,  $Cr_2O_3$ ..), nitridy a karbidy. Na těchto vrstvách se nesmí vyskytovat povrchové defekty, kterými může probíhat difúzní transport a které mohou zcela znehodnotit funkčnost povlaku jako permeační bariéry.

Teoretická část práce je věnována návrhům množivé obálky (breeding blanketu) pro experimentální reaktor ITER, který má jednu část svého programu zaměřenou na problematiku generace tritia v reaktoru a permeační bariéry, materiálům vhodným pro permeační bariéry a technikám vytváření tenkých vrstev z těchto materiálů. Praktická část popisuje experimenty s přetavováním plazmově nastříkaného korundu ( $Al_2O_3$ ) za účelem dosažení homogenního hladkého povrchu bez prasklin a jiných defektů a charakterizaci takto dosažených změn v nástřiku. Klíčová slova: permeační bariéry, TBM, přetavování,  $Al_2O_3$

Permeation barriers are important part of material engineering for the study of controlled thermonuclear fusion. Their aim is to prevent hydrogen isotopes losses, mainly tritium, from the fusion reactor circuit. That would cause fuel and radiation leakage. Principle of barrier manufacturing is the deposition of thin layers of materials with low permeability on the breeding blanket components and other auxiliary systems. These materials involve mainly oxidic ceramics ( $Al_2O_3$ ,  $Cr_2O_3$ ..), nitrides and carbides. The layers must not contain defects, that could enable diffusion through the material and degrade the performance of the barrier.

Theoretical part of this work is focused of breeding blanket designs for ITER, materials suitable for permeation barriers and techniques of deposition capable of forming layers with sufficient parameters. Experimental part follows the experiments of plasma sprayed  $Al_2O_3$  remelting in order to achieve homogenous and smooth surface without cracks and other defects and characterization of thereby obtained changes in the coatings.

Key words: permeation barriers, TBM, remelting,  $Al_2O_3$

## **Acknowledgements**

I would like to thank Ing. Jiří Matějček, Ph.D., for supervising of my thesis, for helping with samples preparation for experimental part and evaluating of the results, for language correction, numerous advices and extra questions. I would like to thank Ing. Jan Čížek, Ph.D. and Bc. Jan Kouřil for invaluable help during experiments on NETME facility on VUT in Brno. Lastly I would like to thank my partner, for great patience and support during writing of the thesis.

# Contents

<b>1</b>	<b>INTRODUCTION</b>	<b>3</b>
<b>2</b>	<b>Breeding blanket designs</b>	<b>5</b>
2.1	Water cooled ceramic breeder . . . . .	6
2.2	Helium cooled ceramic breeder . . . . .	7
2.3	Helium cooled pebble bed . . . . .	8
2.4	Helium cooled lithium lead . . . . .	8
2.5	Dual coolant lithium lead . . . . .	9
2.6	Lithium lead ceramic breeder . . . . .	9
2.7	Water cooled lithium lead . . . . .	10
<b>3</b>	<b>Materials for permeation barriers</b>	<b>11</b>
3.1	$ZrO_2$ . . . . .	13
3.2	$Cr_2O_3$ . . . . .	13
3.3	$Al_2O_3$ . . . . .	13
3.4	$Er_2O_3$ . . . . .	14
<b>4</b>	<b>Fabrication technologies</b>	<b>17</b>
4.1	Physical vapour deposition . . . . .	17
4.2	Chemical vapour deposition . . . . .	18
4.3	Chemical densification coating . . . . .	19
4.4	Hot-dipping aluminization . . . . .	19
4.5	Electrochemical deposition . . . . .	20
4.6	Pack cementation . . . . .	21
4.7	Plasma spraying . . . . .	21
<b>5</b>	<b>Remelting of APS <math>Al_2O_3</math> with the use of electron gun – experimental part</b>	<b>22</b>
5.1	Literature survey . . . . .	22
5.2	Remelting experiments and results . . . . .	26
<b>6</b>	<b>Summary</b>	<b>35</b>

# Chapter 1

## INTRODUCTION

Thermonuclear fusion is a promising source of energy that may be able to resolve the uprising energy crisis. Its benefits involve vast amount of resources, secure service and almost no harmful waste – the product of the reaction intended in International Thermonuclear experimental reactor (ITER) and demonstrational power-plant (DEMO) is only helium, noble gas with no negative effects for the environment. All tritium produced in the reactor will be utilized in the reaction and will not escape the power plant circuit (Figure 1.1), except for undesirable tritium permeation.

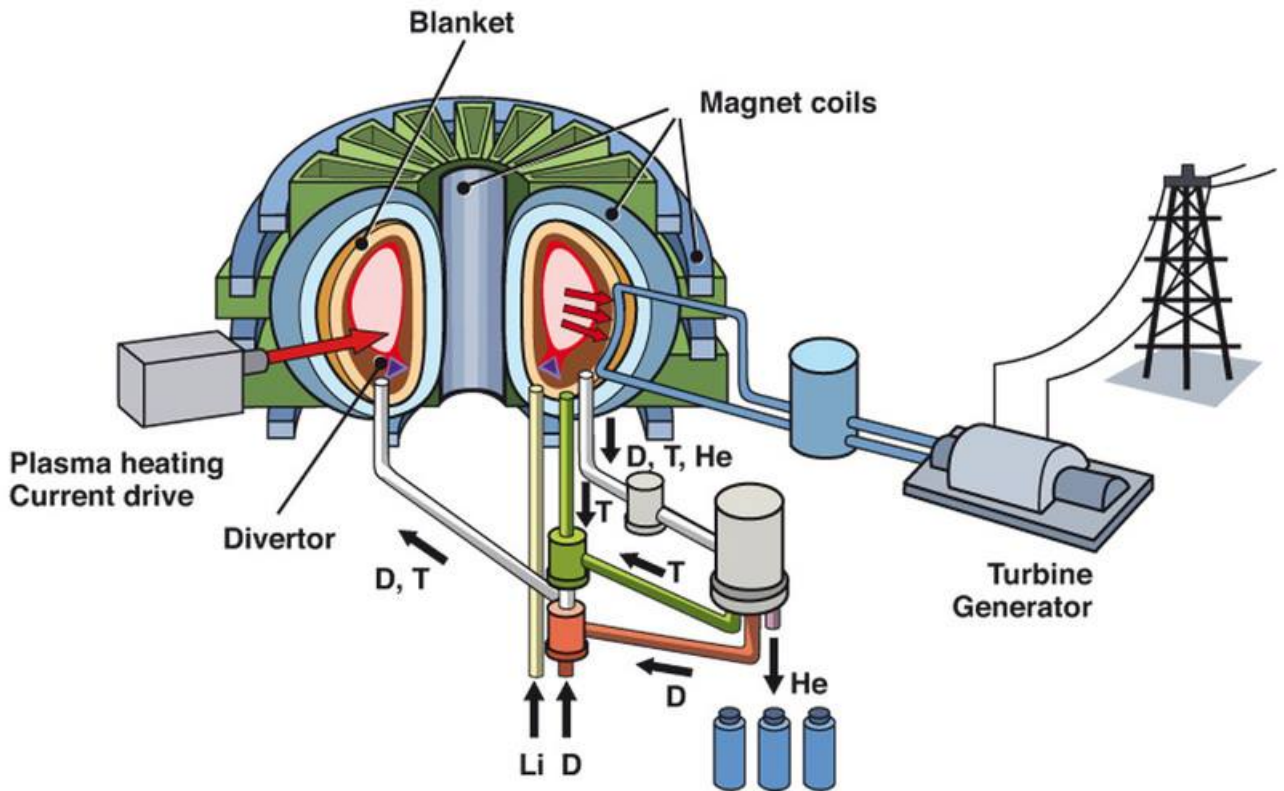


Figure 1.1: Scheme of fusion power plant circuit [1]

However the resulting radiation risk and burden is significantly lower than in fission. These issues are to be solved by material engineering, which is facing great challenge in facilitating thermonuclear fusion as routine energy source not only in this area. In order to provide continuous service of potential reactor, the materials would have to withstand high thermal shocks or neutron fluxes, as well as corrosion environment, for particular parts of the reactor. Very important issue would be tritium management, because in economical and practical

terms, as well as security terms, it would be essential to avoid leakage of radioactive tritium from the breeding area to other circuits of the reactor, or eventually outside the reactor. Therefore, the essential property of materials used in these particular areas is low tritium retention and permeability [2]. Target value of T losses into the environment from the whole power plant circuit is commonly set between 0,6 g and 1 g per year. In comparison with the amount of tritium consumed annually in a 1 GW reactor – slightly over 100 kg, the difference is 5 orders of magnitude. In the matter of T production, expected breeding rate is about 350 g per day and the overall losses should not exceed 2 mg.

This however cannot be achieved by bulk materials that are suitable to form such large-scale structures as reactor parts, with sufficient strength and toughness. Required permeation properties can be fulfilled while providing these base materials (various types of steels) with additional coating, prepared from a material with inherently low tritium permeation. There have been numerous studies concerning this topic recently and suitable materials have been identified: mostly ceramics, e.g.  $Al_2O_3$ ,  $Cr_2O_3$ ,  $Er_2O_3$ , or TiN, TiC, respectively bilayers or trilayers of those above mentioned compounds, prepared by various means – chemical densification coating (CDC), vacuum plasma spraying (VPS), hot-dip coating, cementing etc.

Theoretical part of the thesis consists of research of materials exploitable in permeation barrier fabrication, as well as the fabrication processes. Recent progress in the design and fabrication of tritium breeding modules is discussed from the view of tritium permeation. Experimental part is focused on remelting of plasma sprayed alumina with electron beam. The goal was to eliminate the voids and to improve the permeation barrier function. Literature survey in this field is also included.

## Chapter 2

# Breeding blanket designs

In future fusion power plants, the tritium breeding blanket is going to be essential part of all devices. The primary purpose of breeding blanket is to supply the fusion reaction with tritium. In the first generation of devices, reaction of hydrogen isotopes, deuterium and tritium will be employed, see equation 2.1.



The neutron originated in this reaction possesses energy of roughly 14 MeV (4/5 of the reaction energy) and is further utilised to replenish the supplies of tritium according to the equation 2.2.



The blanket will therefore contain compounds of lithium, a neutron moderator and a multiplier. During the reaction, a particular amount of heat is also produced, which needs to be transferred out of the blanket. Potential permeation of tritium into cooling pipes is undesirable, as well as permeation through the blanket boundaries. These are definitely areas with the highest risk of tritium permeation and demand for use of barrier placement. At present, 6 types of test blanket modules (TBM) are developed. TBM is a mock-up of real future breeding blanket fabricated in the size of one ITER vacuum vessel segment. It will be fully integrated in ITER and should verify the operational reliability and feasibility of particular breeding blanket design without endangering its performance, safety and availability. The main objectives are validation of theoretical predictions concerning:

- Structural integrity
- Tritium breeding, recovery process efficiency and inventory
- Integral performance of blanket

[3] Key parameters that will be the most important in the process of determining the most convenient design, are considered to be the following:

- Safety – especially low short-term activation
- Availability – reliability, lifetime of the components and replacement time
- Tritium issues – inventory and permeation
- Simplicity of fabrication

[3] General properties that should be fulfilled independently on the chosen design feature mainly shielding of the magnets and other structural parts, tritium self-sufficiency and compatibility with the remaining reactor systems (cooling loop etc.). During the experiments, all TBMs are going to be installed simultaneously, therefore the figure of merit of various designs can be determined. The TBM consists of first wall, identical as for the rest of the device, only recessed in width, and complete facility to generate tritium and transfer the heat – so called breeding zone. Difference of each version of TBM concerns design of internal systems and required operational conditions. Operational conditions to be reached in ITER are not comparable with those in DEMO. The neutron first wall load is approximately 30 % of DEMO values and neutron fluence is significantly lower. Moreover, experiments performed in ITER will have pulsed character, with short duration compared to quasi-continuous or steady state

operation of DEMO. Despite this, studies have shown, that reliable data can be acquired from TBM testing in ITER, providing that DEMO BBs use the same structural and breeding materials and are designed using proper engineering scaling. Several of these designs feature liquid lead with lithium component, which implies the need of improved corrosion resistance. The list of potential breeding blankets is the following:

- Water cooled ceramic breeder - WCCB
- Helium cooled ceramic breeder - HCCB
- Helium cooled pebble bed - HCPB
- Helium cooled lithium lead - HCLL
- Dual coolant lithium lead - DCLL
- Lithium lead ceramic breeder – LLCB
- Water cooled lithium lead - WCLL

In all designs, Reduced-Activation Ferritic/Martensitic steels are used as structural material. One of the most important features of every breeding blanket is the type of tritium breeder. Division of the blankets, based on the breeder type, is the following:

- Lithium-lead based blankets
- Ceramic based blankets

Lithium-lead based blankets operate with liquid metal eutectic Pb – 17Li (17 %lithium). The use of Pb-17Li is promising, because of its high tritium breeding capability, relatively large thermal conductivity and immunity to irradiation damage. These properties can lead to tritium self-sufficiency and to dropping out of the neutron multiplier. Additionally, it offers unlimited lifetime of the breeder material and therefore the liquid breeder can be re-used in a new facility, after the structural parts of the power station come to end of their operational lifetime. The use of Pb-17Li also allows the establishment of self-cooled configuration of the TBM. However in this case one needs to electrically insulate the Pb-17Li from the walls, otherwise significant magneto-hydrodynamic pressure drop takes place. This is particularly difficult in the area of first wall, therefore the option with He-cooled FW and self-cooled breeding zone was taken into consideration. The MHD pressure drop is also suppressed, when He or water is used as a coolant for whole TBM. Ceramic blankets operate with pebble beds or sintered blocks of lithium compounds, candidates include (in the order of decreasing lithium density):  $LiO_2$ ,  $Li_4SiO_4$ ,  $Li_2TiO_3$  and  $Li_2ZrO_3$ . Be is used as neutron multiplier. Major issues associated with ceramic breeder concepts can be summarized as follows:

- Chemical compatibility between multiplier and coolant
- Tritium production, release and trapping characteristics of breeding materials and multiplier
- Tritium permeation
- Thermo-mechanical interactions between the pebbles and structure
- Limits on power density – low thermal conductivity of ceramics
- Limits on reactor lifetime – neutron irradiation
- Neutron shield performance
- Cost of fabrication and re-processing – enrichment of Li, re-processing of replaced blanket modules

[3]

## 2.1 Water cooled ceramic breeder

WCCB breeding blanket is formed by 2 identical sub-modules, as seen in figure 2.1. F82H steel is used as structural material,  $Li_2TiO_3$  is used as tritium breeder and beryllium pebble beds work as neutron multiplier. Li is enriched 30 % in  $^6Li$ . Coolant water is supposed to flow under similar conditions as in the pressurized water reactor (fission). The use of supercritical water is also under consideration, in order to increase the power cycle efficiency up to 40-45 %. That would however lead to the need of stronger steels as structural materials.

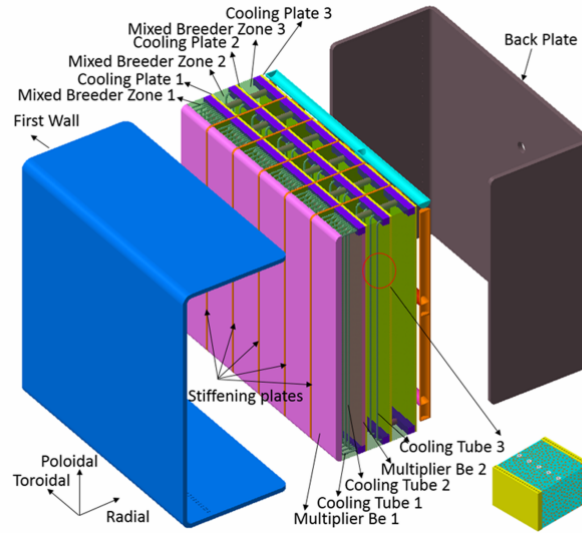


Figure 2.1: Helium cooled ceramic breeder [4]

## 2.2 Helium cooled ceramic breeder

The main components of HCCB TBM are: first wall, manifolds, attachments, cooling pipes and purge gas pipes (2.2). RAFM steel act as structural materials,  $Li_4SiO_4$  pebble beds are used as tritium breeder, beryllium pebble beds serve as neutron multiplier. The whole structure is cooled by helium. Internal structure is the following: the whole space between first wall and back plate is arranged as the breeding zone, it is filled by sequences of poloidal rows of coolant channels, of  $Li_4SiO_4$  and beryllium pebble beds. Be is used as binary pebble-bed, whereas Li as single pebble-beds, with diameter between 0,5 mm and 1 mm. Li in enriched 80 %in  $^6Li$ . Maximum temperatures reached are 900 °C in ceramic, 600 °C in Be and 550 °C on steel. The HCCB design requires several ancillary systems, most importantly the helium purification system.

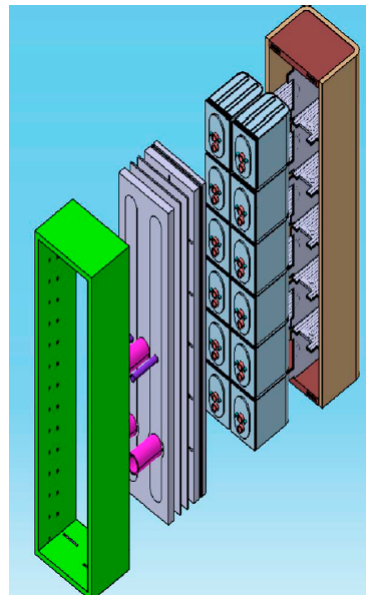


Figure 2.2: Helium cooled ceramic breeder [5]

## 2.3 Helium cooled pebble bed

Structural material used for HCPB BB is Eurofer steel. Two possible compounds act as tritium breeder –  $Li_4SiO_4$  or  $Li_2TiO_3$ .  $Li_4SiO_4$  is enriched 30% in  ${}^6Li$ , whereas  $Li_2TiO_3$  is enriched 60%. Beryllium pebble bed is used as neutron multiplier. Helium, at a pressure of 8 MPa, is used as coolant, with inlet temperature of 300 °C and outlet temperature of 350 °C. Maximum temperature reached in the ceramic is 920 °C, respectively 650 °C in Be and 550 °C in steel. The internal structure of breeding blanket is shown in figure 2.3: it consists of a He cooled box, reinforced in steel grid. Breeder units are inserted in this grid and several plates including the grid, cooled by He, ensure the heat transfer from the tritium breeding. Additional coating to reduce or prevent tritium permeation to the coolant is required. Breeding material and multiplier are compatible with the structural material up to the temperatures, limited by the strength consideration of the support structure. That compatibility, along with additional compatibility with the coolant is the main advantage of HCPB breeding blanket.

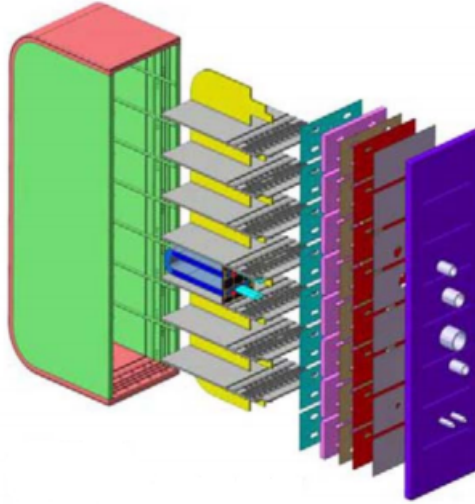


Figure 2.3: Helium cooled pebble bed [1]

## 2.4 Helium cooled lithium lead

HCLL BB is molten liquid based breeding blanket design. Internal structure is shown in figure 2.4. Liquid Pb-16Li, enriched 90% in  ${}^6Li$ , is used as tritium breeder as well as neutron multiplier. Eurofer steel is used as structural material. Helium is used as a coolant, inlet temperature is 300 °C, outlet temperature is 500 °C. Operational temperature of steel structures reaches up to 550 °C and at these levels, severe corrosion attack from direct exposure of the steels to liquid Pb-Li occurs. Calculations have shown the corrosion attack of 400  $\mu m$ /year, it means 4 kilograms/square meter/year of material dissolved from the structures. It is a significant amount of material that could cause tube plugging or even break the integrity of blanket. To provide safe operation, it has been decided to coat the endangered areas with protective Al based layers. Because of unsatisfactory results of chemical vapour deposition, vacuum plasma spray or hot-dip aluminization, electrochemical deposition (ECA/ECX) was chosen. Using ECX, 10  $\mu m$  Al layer was successfully deposited. The coating was homogenous even on complex shaped structures and exhibited very good performance in testing. The corrosion test ran for 5300 hours at various temperatures (350 °C – 550 °C) and 0,22 m/s Pb-Li flow and no corrosion losses were measured [6, 7]. Maximal value of lost tritium (due to the permeation) is estimated to 1 g/day, to fulfil feasibility and safety of the reactor. To ensure this, particular areas of breeding blanket and following circuit have to be provided by permeation barriers. The exact values of PRF are difficult to estimate, because of conditions that are uneasy to determine, but Gastaldi et al [7]. stated that blanket coating should have PRF values up to 100 and steam generator up to 200, exceptionally up to 400 is required.

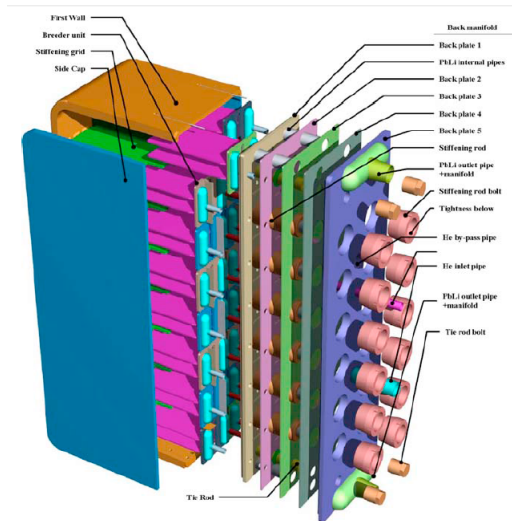


Figure 2.4: Helium cooled lithium lead [5]

## 2.5 Dual coolant lithium lead

DCLL breeding blanket uses helium as coolant for first wall and structural part. Pb-16Li acts as tritium breeder, as well as neutron multiplier and secondary coolant. Li is enriched at 90 %in  ${}^6\text{Li}$ . Pb-Li circulates from back to front at a velocity roughly 10 m/s. The outlet temperatures of Pb-Li can reach up to 700 °C. In the range of these temperatures, efficiency of 45 %is achievable. Electrically and thermally insulated steel plates are cooled with helium and act as a flow separator of Pb-Li (figure 2.5). The inlet temperature of He is about 350 °C, the outlet temperature about 410 °C. Temperatures in the structures reach up to 550 °C, while in SiC up to 600 °C (SiC acts as thermal insulator). As well as HCCB, the DCLL design requires several ancillary systems, most importantly the helium purification system and tritium extraction system.

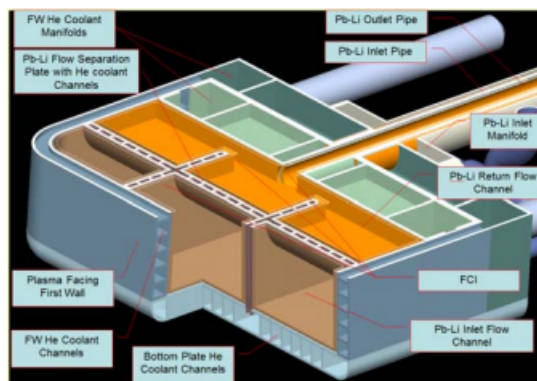


Figure 2.5: Dual coolant lithium lead [1]

## 2.6 Lithium lead ceramic breeder

LLCB BB combines features of ceramic and lithium lead based concepts. Structural materials are RAFM steels. The internal structure is showed in figure 2.6. Both  $\text{Li}_2\text{TiO}_3$  pebble bed and Pb-16Li act as tritium breeder. Pebble beds are enriched by 30-60 %in  ${}^6\text{Li}$  and by 90 %in Pb-16Li. The Pb-Li serves simultaneously as coolant for ceramic breeder beds and neutron multiplier. Helium acts as an additional coolant, it is purged under pressure of 8 MPa, with inlet temperature of 300 °C and outlet temperature of 350 °C.

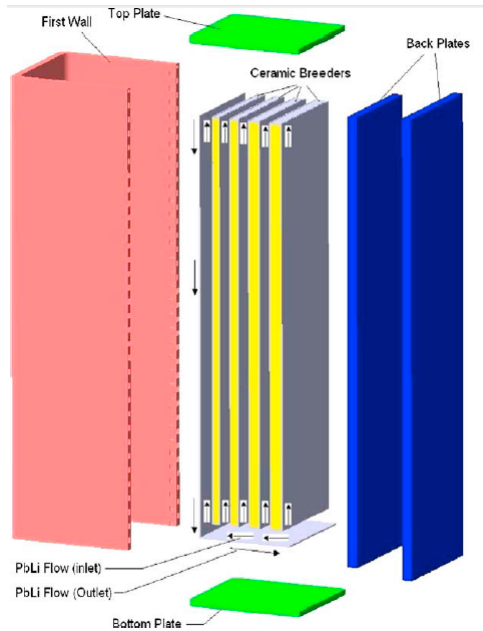


Figure 2.6: Lithium lead ceramic breeder [5]

## 2.7 Water cooled lithium lead

WCLL BB use experiences gained during the operating of PWR reactors. Two independent coolant circuits, one for the first wall, second one for the breeding zone, are used to improve safety of the reactor (figure 2.7). Both are using water. EUROFER steel was chosen as structural material. Drawbacks of this concept are low thermal efficiency – 33 % and control of Pb-Li/water interaction and permeation of T from Pb-Li to water. That can be solved by several means – appropriate dimensioning of the Pb-Li container, using double wall coolant tubes and applying T permeation barriers on the tube surfaces. For a complete list of options, breeding

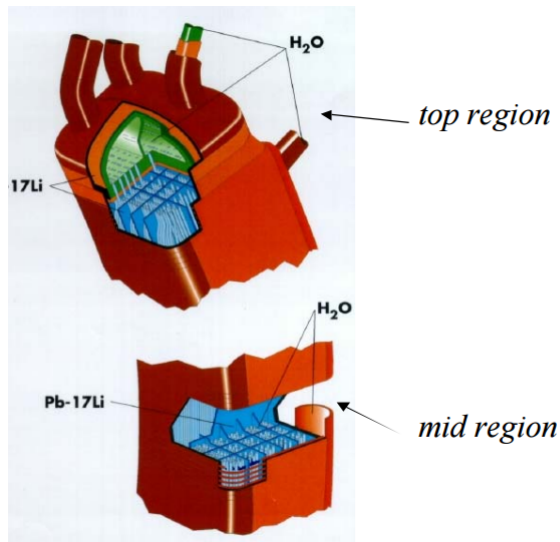


Figure 2.7: Water cooled lithium lead [8]

blankets with SiC as structural material, tungsten based concepts and concepts using FLiBe as tritium breeder were taken into consideration, however they are not included in the ITER programme.

## Chapter 3

# Materials for permeation barriers

Materials suitable for providing protective layer on the structural material of TBM can be identified through some essential characteristics that they need to fulfill. The choice of particular elements stems out of the principles governing the tritium permeation and the facility requirements. The fundamental property must be obviously inherently low tritium permeability [9]. Effectiveness of the material as a permeation barrier is often assessed by the PRF – permeation reduction factor. It is a ratio of permeability of specimen with permeation barrier to an equivalent bare specimen, without the barrier. Previously reported values of PRF from laboratory experiments reached up to several thousand [10, 11, 12, 13, 14, 15], however other measurements also proved that PRF drops significantly in radiation environments and when exposed to liquid breeder material (Pb-Li). Experiments performed in Netherlands already showed that in that case, PRF values did not exceed 100 [16, 17, 18, 19, 20]. Hydrogen can permeate through the material either by dissolving in the material or by diffusion through holes, cracks, pores or other imperfections. In case of dissolving, which occurs when there are no imperfections in the surface layer or their surface density is low, the permeation involves multiple steps:

- Diffusion of permeating species from bulk fluid to material surface in response to a concentration gradient.
- Adsorption of species onto material surface by physisorption, chemisorption, or chemical reactions. This may involve the decomposition of the adsorbing species into subelements.
- Absorption of permeating species or sub-elements of these species into the solid material and diffusion of the permeating species or sub-elements of these species across the bulk material in response to a gradient.
- Re-emergence of the permeating species or sub-elements of these species on the opposite surface (desorption and recombination).
- Diffusion of permeating species or sub-elements from the opposite surface into the bulk fluid on the other side of the solid material in response to a gradient. If sub-elements are released freely, then the solid material is acting as a reactive membrane; otherwise the sub-elements must first recombine into the original permeating species before being released.

[9] These processes occur at different rates, and each of these steps can be the rate-limiting process. The process is schematically shown in figure 3.1.

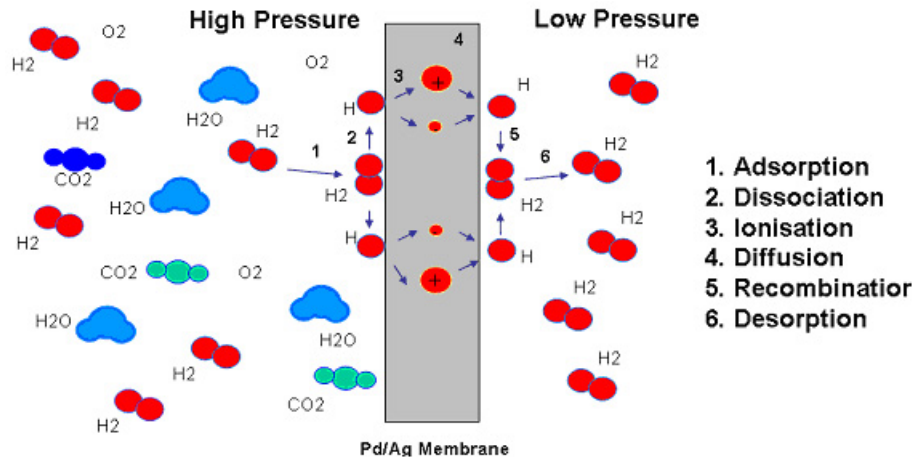


Figure 3.1: Hydrogen permeation through the material [21]

Possible imperfections in surface layer enable the permeating gas to evade this more demanding way of transport, or shorten the distance necessary to overcome by diffusion. Materials selected for permeation barriers possess properties that effectively lower the permeation rate through intact surface. Dominant contribution to permeation flux through material is therefore permeation through voids, cracks and other imperfections in the protective layer. Therefore to minimize the permeation rate, the selected material should be able to form dense and homogenous layers without defects. In order to prevent degradation of the surface by peeling of significant fraction of the layer, good adhesion and chemical compatibility with the substrate material is required. During future operation, the permeation barrier will have to withstand significant thermal shocks, heat and neutron fluxes – operational temperatures can reach up to 550 °C in steels and up to 900 °C in other materials, while coolant inlet temperatures vary between 280 °C to 350 °C, heat fluxes are considered to be 0,2 - 1  $MW/m^2$  and neutron loading 1,5 -10  $MW/m^2$ , depending on the blanket design. In case of liquid breeder TBM, corrosion resistance would become a non-negligible aspect, too. Due to irradiation from fusion neutrons and tritium production, the permeation barrier would become activated and radiation damaged. Replacement of the blanket modules would be connected with great difficulty and hazard, therefore the potential in-situ self-healing ability would be beneficial in the choosing procedure. In addition to above mentioned physical criteria, one has to consider the availability of particular material and expenses of coating of complex surface of industrial scale facility. Issues that are discussed in order to determine the suitability of the particular compound are therefore the following:

- Ability to reduce permeation of tritium – assumed values of TPRF are over 1000 for gas phase tritium and over 100 for liquid Pb-Li
- Adhesion to substrate material
- Chemical compatibility with substrate material
- Material availability/cost
- Radiation damage/thermal shocks/corrosion resistance
- Potential for self-healing

[22, 23]

The range of materials that have recently been investigated include mostly ceramics, e.g.  $Al_2O_3$ ,  $Cr_2O_3$ ,  $Er_2O_3$ . Other compounds that have been taken into consideration are TiN or TiC, several experiments with use of NiAl and FeAl were also conducted. Particular effort was put into experiments with multiple layers of all mentioned materials. Investigation on further improvement of permeation reduction factor were performed on such treated samples.

### 3.1 $ZrO_2$

Zirconia is a favorable material for anti-permeation coating, due to similarity in thermal expansion coefficient with steels. In addition, zirconium is a low-activation element [24].

### 3.2 $Cr_2O_3$

It has been shown that  $Cr_2O_3$  is a promising material for barrier application because of its properties. It is thermally stable at high temperatures, even exceeding 1273 K, chemically inert, is not susceptible to oxidation [25] and its dissociation pressure is low [9]. Therefore is it allowed to form at elevated temperatures and low oxygen partial pressures. Permeation reduction provided by chromia oxides reaches up to two orders of magnitude (figure 3.2), however during the deposition, various  $Cr_2MO_4$  spinels may form, which have lower PRF [26]. Chromia acts also as a part of mixed oxides that, deposited by chemical densification, are able to provide permeation reduction of four orders of magnitude [27].

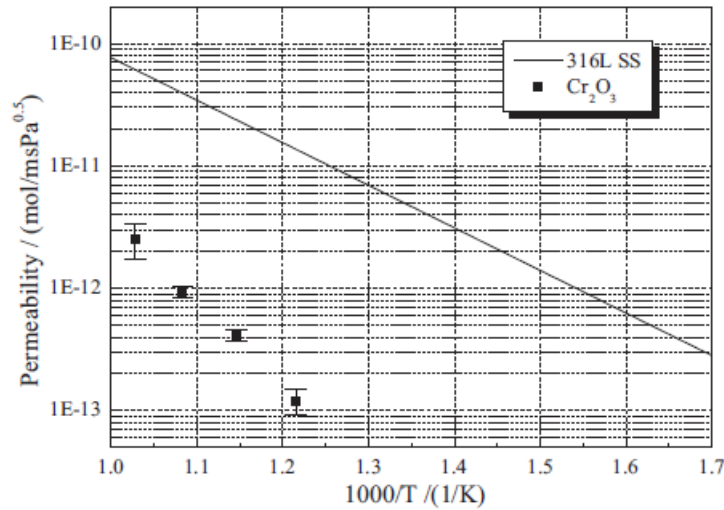


Figure 3.2: Temperature dependence of permeability through bare 316L steel sample and reduction after coating with  $Cr_2O_3$ [25]

### 3.3 $Al_2O_3$

$Al_2O_3$  was first proposed material for permeation barriers, because of high permeation reduction factor, good thermodynamic property, self-healing ability etc. [28]. Stability of Al coating and the ability to re-form at low oxygen partial pressures were confirmed. The reason for these properties is very high free energy of oxide formation of the Al [29]. Examples of permeation reduction up to three orders of magnitude after applying  $Al_2O_3$  coating are shown in figures 3.3 and 3.4. Numerous permeation tests were performed before and it was stated that  $Al_2O_3$  is able to suppress permeation rate of deuterium up to 3 orders of magnitude [31]. However alumina may form several phases during crystallization. Favourable for barrier fabrication is the corundum phase ( $\alpha - Al_2O_3$ ) that forms at temperatures above 1373 K. This phase is thermodynamically stable with sufficient hardness and permeation properties. However such high temperatures might negatively influence properties of substrate material [30]. Suitable deposition methods of  $Al_2O_3$  are numerous – plasma spraying, pack cementation, chemical vapour deposition [31]. Sufficient corrosion and T-permeation protection of CVD, VPS or HDA samples were identified. Compatibility testing at high temperatures was also successful. Major drawbacks were, however, lack of ability to coat complex parts and high amount of aluminum needed for the deposition. As a technique that would better fulfill requested criteria – homogenous deposition, controllable and adjustable thickness, and industrial relevance – electrochemical deposition (ECA/ECX) was identified. ECA stands for specific deposition of aluminum, whereas ECX is capable to deposit whole range of other elements. Unfortunately, in the case of aluminum, the use of nonaqueous electrolytes is required, due to high

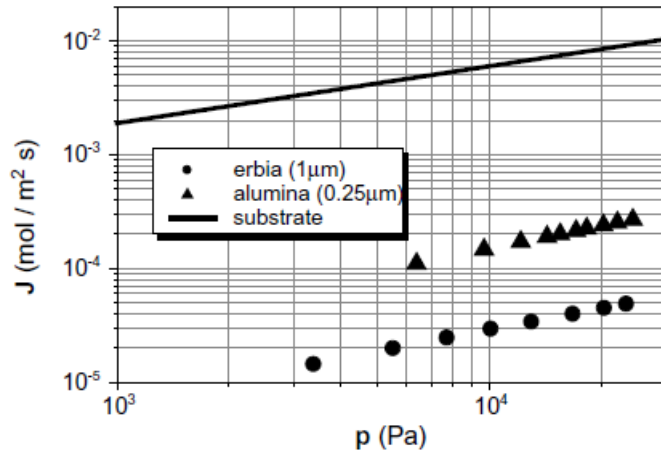


Figure 3.3: Permeation reduction of thin  $Al_2O_3$  and  $Er_2O_3$  films [30]

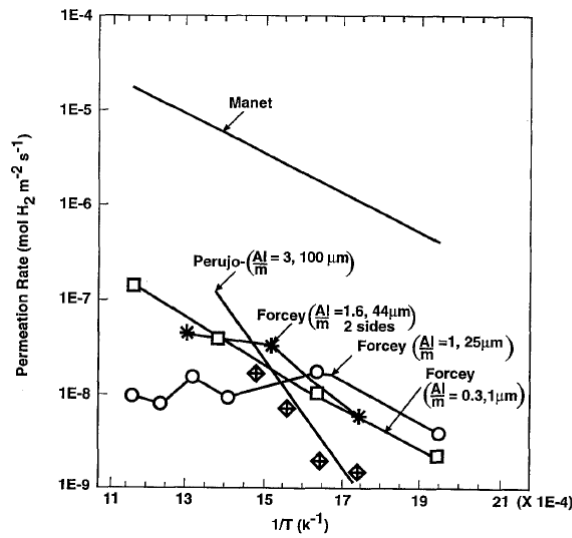


Figure 3.4: Permeation rates through  $Al_2O_3$  coated MANET [29]

electronegativity of aluminum. Using these electrochemical techniques, layer thickness can reach as low as several micrometers with the use of 10 times lower aluminum amount [6].

### 3.4 $Er_2O_3$

$Er_2O_3$  is also among preferable materials for coating plant-relevant surfaces. Successful deposition of  $Er_2O_3$  through number of techniques showed thermal and mechanical stability of the coating [9], corrosion resistance in contact with liquid PbLi [30] or low deposition temperature [32]. In particular areas, the results are better than in case of using of  $Al_2O_3$ . For example  $Er_2O_3$  shows better compatibility with liquid Pb-Li at higher temperatures [28]. Metal organic chemical vapour deposition (MOCVD) [33] (figure 3.5 and 3.6), physical vapour deposition (PVD) [34] or dip coating [35] (figure 3.7) were identified as deposition techniques, suitable for  $Er_2O_3$ .

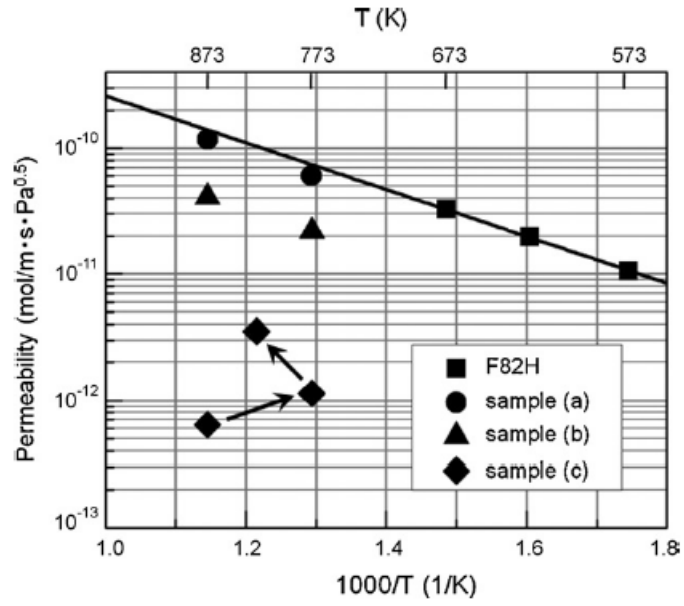


Figure 3.5: Temperature dependance of permeability through erbium oxide layer [33]

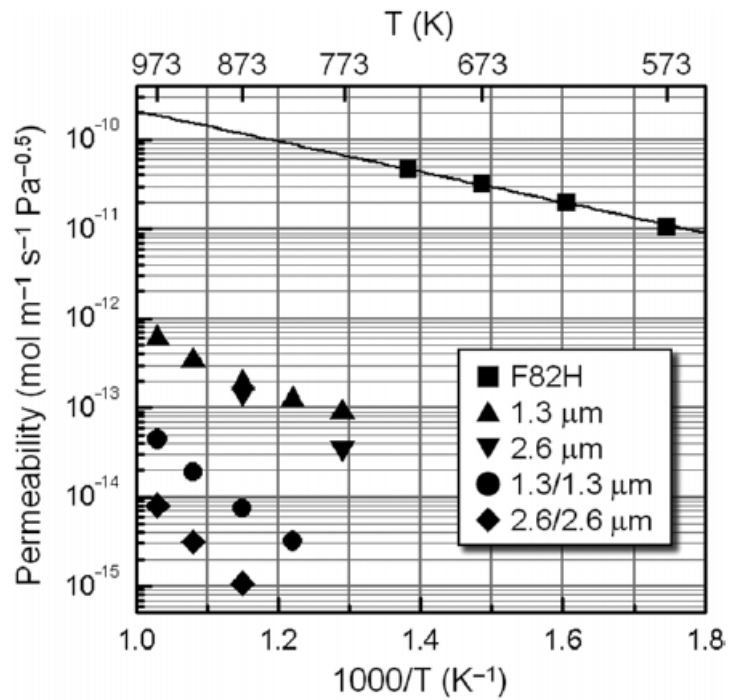


Figure 3.6: Temperature dependance of permeability through F82H steel using one side/two side erbium oxide coating [33]

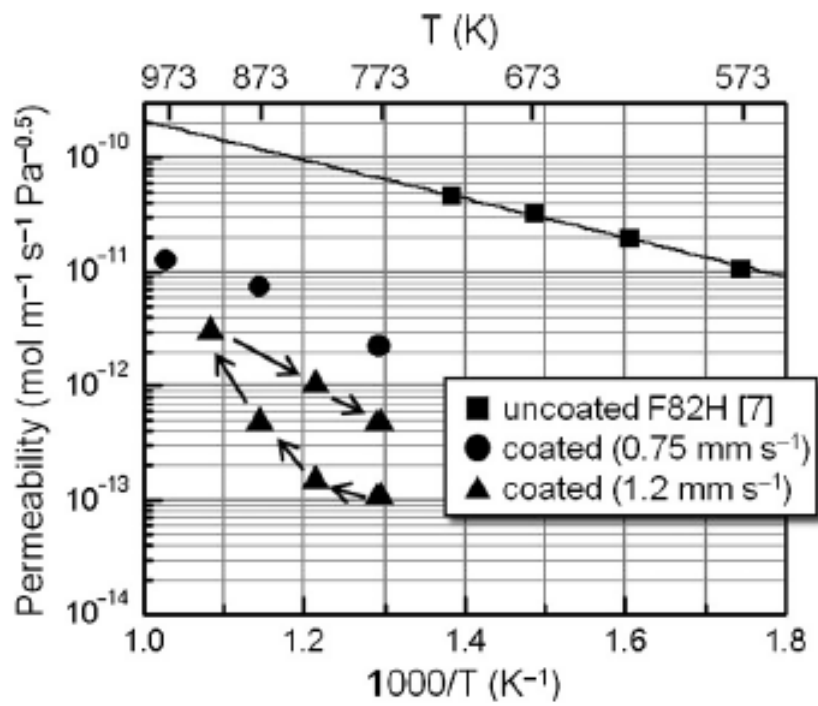


Figure 3.7: Temperature dependence of permeability through erbium oxide layer [35]

# Chapter 4

## Fabrication technologies

In order to determine reliable way of tritium barrier fabrication suitable for laboratory scale experiments as well as future transition to industrial relevant form, numerous different techniques were investigated. These consisted of:

- Physical vapour deposition - PVD
- Chemical vapour deposition - CVD
- Hot dip aluminization - HDA
- Electro chemical deposition - ECD
- Pack cementation - PC
- Plasma spraying - PS
  - VPS - vacuum
  - APS - atmosphere
- Chemical densification coating - CDC
- Metal organic chemical vapour deposition - MOCVD

Particular experiments that were performed, along with the data obtained are shown below the overall characteristics of each method. Generally, all above mentioned methods vary in physical principles, conditions required for sufficient performance, e.g. temperature, usable materials, etc. In terms of potential suitability for barrier production, the following criteria are examined:

- Ability to deposit desired material
- Ability to form dense and homogenous layers without defects
- Potential for coating large complex configuration

[23, 36]

### 4.1 Physical vapour deposition

PVD is a technique of deposition of source material through its conversion into gaseous atoms. This is done via evaporation, sputtering or ionization. Deposited particles form coatings or films of thickness approximately micrometres. Experiments validated the availability of PVD to form TPB. Perujo et al. [31] deposited 1,5  $\mu\text{m}$   $\text{Al}_2\text{O}_3$  coating on MANET steel by magnetron sputtering. Deuterium permeation was then measured at 300 – 500 °C and maximum decrease was of about 4 orders of magnitude, compared to uncoated sample. Experiments with plasma assisted PVD coatings of  $\text{Al}_2\text{O}_3$  and  $\text{Er}_2\text{O}_3$  were performed by Koch et al. [30]. The coatings differed in composition and also in thickness. 0,25  $\mu\text{m}$  coating of  $\text{Al}_2\text{O}_3$  reached PRF values of 40. 1  $\mu\text{m}$  coating of  $\text{Er}_2\text{O}_3$  reached PRF values of 200 and after detailed investigation, it was found that the coating was stable in contact with Pb-Li and kept the PRF values after neutron irradiation. During some experiments, however, difficulties with PVD occurred. The coating was nonuniform, exhibited poor bonding to the substrate and an easy fall-off. Complex geometric surfaces were difficult to coat too.

## 4.2 Chemical vapour deposition

CVD is a process when solid film on the substrate forms via gas phase or after particular chemical reactions. Elementary substance or compound is first introduced to the substrate by film composing element, and then particular reaction takes place. This process possesses some advantages, such as simple facility required, continuous and controllable film composition, uniform and dense surface, and availability of complex-geometry coating.

Experiments with CVD technique were performed by Benamati et al. Fe-Al coating was deposited on martensitic steel, using some beneficial steps: a) using (Al,Fe) donor, b) low pressure deposition, c) testing the deposition at temperatures below 1023 K. As a result, the deposited layer was very dense, no crack or porosities occurred, and excellent adhesion was reached. The values of PRF were not measured [37]. Matejicek et al. conducted experiments with Al based coatings fabricated by CVD or HDA following CVD. Steel plates and tubes were used as substrate, resulting PRF values were  $> 10^3$  for plates in gas phase, but  $< 10^2$  when exposed to Pb-Li. In case of tubular specimen and HDA following CVD, measured PRF was 9 – 98 [22]. Similar experiments were performed by Aiello et al., 1 mm thick tubular specimen were coated by CVD with  $Al_2O_3$  and resulting PRF values were 9 - 25 for gas measurements, 8 - 20 for Pb-Li measurements [38]. Forcey et al. performed experiments on planar specimens and capsules. Internal bilayer of  $Al_2O_3$  on TiC in total thickness of 3  $\mu m$  was deposited on steel capsule. Permeation reduction reached 1 order of magnitude and coating was resistive to Pb-Li, after exposure, no effect on permeation reduction was observed. In another series of experiments, additional 80  $\mu m$  internal layer was prepared by pack cementation (see below). Permeation reduction in this case reached 2 orders of magnitude and its increase over time was observed, probably due to in-situ oxidation. However, exposure to the Pb-Li completely degraded the sample, no permeation reduction was measured. Post-experimental investigations revealed presence of large number of cracks in the coating and bad adhesion to the substrate [39].

Permeation measurements were performed on TZM steel and 316L steel disk samples. Deposited compounds were TiC, bilayer of TiN and TiC, and trilayer of TiC, TiN and  $Al_2O_3$ . TZM substrate was 0,1 mm thick, layers of TiC were 1  $\mu m$ , respectively 2  $\mu m$ . 316L samples were 1 mm thick, bilayer of TiC and TiN was 3  $\mu m$  in total, trilayer consisted of 4  $\mu m$  of  $Al_2O_3$  on 2  $\mu m$  of bilayer. TiC coating on TZM steel was less effective as expected, 1  $\mu m$  thick layer reached 1 order reduction, even though from already measured data, TPRF should reach values  $10^3$ . 2  $\mu m$  coating was not effective at all due to the presence of cracks. Bilayer of TiN and TiC on 316L steel reached TPRF of one order, additional layer of  $Al_2O_3$  did not improve the results. Because  $Al_2O_3$  is usually considered as very promising material and its ability to reduce permeation is very high, it was thought, that the deposited layer must have contained defects that degraded the performance [40]. On the other hand, CVD requires certain temperature for successful deposition and this temperature is mostly unfavourable for the mechanical properties of structural materials. Therefore, some advanced techniques on the basis of CVD were developed, in particular metal organic CVD (MOCVD) and CVD in fluidized bed reactors (CVD-FBR). Both these methods require lower temperatures for the coating. CVD, MOCVD and also CVD-FBR were verified by Natali et al. [41]. By MOCVD, an  $Al_2O_3$  scale was prepared, with some impurities of carbon and hydrogen. Temperature needed for deposition was 653 K and the elimination of impurities is possible, e.g. by altering the Al source or using the way of gas carrying. Aluminide coating prepared by CVD-FBR on P-92 steels was about 8  $\mu m$  thick. The growth rate and composition of coating depended on reactive gas and deposition time. FeAl/ $Al_2O_3$  coating was prepared by two-step method - CVD/CEA. Permeation measurements were performed in air, as well as in liquid Pb-Li. Reduction factor in air was 6, while in liquid Pb-Li, value of 15 was reached [36]. Experiments with  $Cr_2O_3$  coating using MOCVD technique were performed. The metal-organic precursor (chromium acetylacetonate) was heated to 433 K to evaporate,  $H_2$  was chosen as a carrier gas, reaction gas was  $H_2O$  vapour. Final coating was dense and homogenous, crack and carbon free, with corundum  $Cr_2O_3$  structure. Measured values of PRF were 24 – 117, depending on temperature (24 at 973 K, 117 at 823 K) [25]. Xiang et al. [36] therefore stated, that CVD methods are promising, but there is still a long way to engineering application.

### 4.3 Chemical densification coating

CDC is a deposition technique that consists of substrate pretreatment, coating with slurry and heating. The slurry contains compounds desirable to form the protective layer. Final densification is performed by impregnation of the sample with acid solution. The solution again consists of compounds of future protective layer. During experiments with various techniques of permeation barriers fabrication, CDC coating of  $Cr_2O_3$ - $SiO_2$  was investigated. The coating was prepared at low temperature and although some pores in the surface appeared, they were sealed with  $Cr_2PO_4$  where necessary. Afterwards measured PRF reached 1000 [42].

### 4.4 Hot-dipping aluminization

HDA is a TPB preparation technique, in which the substrate is dipped into melted aluminium. Time of dipping is chosen in order to ensure complete wetting of surface, but at the same time to minimize the amount of aluminium reacting with the substrate. HDA is promising for the stability, homogeneity and compactness of coating. Lab-scale MANET II samples were HDA treated – dipped into Al melt and thermally oxidized. Maximum obtained values of deuterium PRF were 260 at 743 K and 1000 at 573 K. However during some permeation measurements, there was a great deviation of PRF in air and in liquid Pb-Li. Values of PRF of MANET II container in the range of temperatures 573 – 823 K was 140 in air, but only 45 in liquid Pb-Li. Experiments with various temperature of molten Al were performed by Shi et al. Deposition temperatures were 1033, 1073 and 1123K, temperatures of post treatment were 923, 1123, 1323 K. It was detected, that along with the temperature, the deposited coating is thicker and the amount of  $Fe_2Al_5$  is rising. TPRF in air reached the values  $> 10^3$ , while in liquid Pb-Li  $> 10^2$ . The investigation of the coating also declared Li-compatibility, corrosion resistance, good thermomechanical integrity, large component coating availability and in-situ self-healing ability. These properties were maintained even in the presence of high temperatures and magnetic fields [43]. In order to provide permeation protection for cooling tubes in WCLL TBM design, Aiello et al. performed experiments using HDA and CVD. 1 mm thick tubular specimen were coated and resulting PRF values in case of HDA were 30 – 100 for gas measurements, 17 – 45 for Pb-Li measurements [38].

Chikada et al. discussed experiments of  $Er_2O_3$  coatings. They reported early experiments with following results: 0,3  $\mu m$  coated sample (disks) – PRF 500-700, 1  $\mu m$  both sides dip-coated sample – PRF up to  $10^2$ . The difference in permeation reduction was assigned to substrate surface conditions. The both sides coated sample surface was oxidized and further observations showed pores in the coating. Experiments performed by Chikada et al. consisted of dipping into precursor containing  $Er_2O_3$ , slowly withdrawing with velocities of 0,05 – 1,5 mm/s and drying at 393 K for 10 minutes. This procedure was repeated, until the gravity induced unevenness of surface was reduced. After a sufficient number of cycles, additional heat treatment was performed to crystallize  $Er_2O_3$  coating. In total 3 samples were examined. Sample 1 was withdrawn at 0,75 mm/s and the PRF values reached 20 – 30 at temperatures of 773 to 923 K. Sample 2 was withdrawn at 1,2 mm/s, the PRF values reached 600 – 700, although the surface was not completely crystallized. Sample 3 was withdrawn at 1,2 mm/s too, but it was double processed compared to sample 2. Therefore the PRF values were  $10^3$ . Coating was deposited also on steel tubes and the procedure was repeated 3 times, resulting in 0,3  $\mu m$  coating on both inner and outer surface. Permeation measurements were performed at low tritium partial pressures – 1,2 ppm (0,13 Pa)/ 40 ppm (4,2 Pa) and temperatures from 670 to 1020 K. Below 870 K the permeation signal was undetectable. At higher temperatures, permeation was reduced by 2 orders of magnitude, compared to uncoated sample, both at 1,2 ppm and 40 ppm [35].

Glassbrenner et al. performed experiment of HDA coating on MANET II steel substrate. The samples were 1,2  $\mu m$  thick and Al contained minor impurities of Mg, Mn and Fe. In addition to standard HDA deposition, the coated samples underwent additional oxidation for 10, respectively 30 hours, and hardening. As a result, the sample after 10 hours oxidation reached permeation reduction of 2 orders and better adherence than second sample which, on the other hand managed to reach the reduction of 3 orders. Both samples contained minor delamination and spallation, probably due to the presence of Mg [44]. Moreover voids and cracks tend to appear in the coatings. These imperfections degrade the barrier performance, and therefore steps to eliminate such processes have to be taken. This can be achieved by using HIP – hot isostatic pressing or by using doping elements, e.g. doping with rare earth elements can efficiently suppress formation and growth of imperfections.

## 4.5 Electrochemical deposition

The ECD technique requires simple facility that is easy to operate, moreover the thickness and composition of coating is controllable. By varying the current density and time, thickness from nanometres to millimetres can be achieved. Along with the capability to coat complex-geometry surfaces and low temperatures below 100 °C, ECD is very promising in the TPB preparation. ECD technique requires the use of electrolytes during the deposition. These electrolytes differ with the compound that is to be deposited on the substrate. Electro deposition of Al can be conducted only in aprotic electrolytes due to its high electronegativity. This process is named ECA and organic aprotic electrolytes are used. Electrolytes used in ECA are highly volatile and therefore the coating has to be done in a protective environment. Deposition of other elements (e.g. W, Ta, etc.) requires the use of ionic liquids (IL) and the process is named ECX. IL possess particular features that favour the use of ECX: great thermal and chemical stability, low vapor pressure, high electrical conductivity, high variability of chemical structure, good miscibility with inorganic metal salts and liquid at room temperature. Experiments have also shown that ECX produced smoother layers and finer grained coating than ECA. 20  $\mu\text{m}$  thick, dense and well adherent FeAl coating was prepared on steel samples with ECX. This proved the ability to coat with ECX technique, however the coating performance was not satisfying. To enhance the PRF, ECX has to be combined with post-treatment processes such as oxidation, annealing or HIP treatment. After this combined treatment, PRF can be increased by at least one order of magnitude. Zhang et al prepared FeAl/ $\text{Al}_2\text{O}_3$  coatings on stainless steel containers. Measurements showed the deuterium PRF of 3000 at 773 K and 100 at 1113 K [36]. Arc discharge technique was used in experiments with various types of ferritic or martensitic steels, e.g. SS316, SS430 or JLF-1.

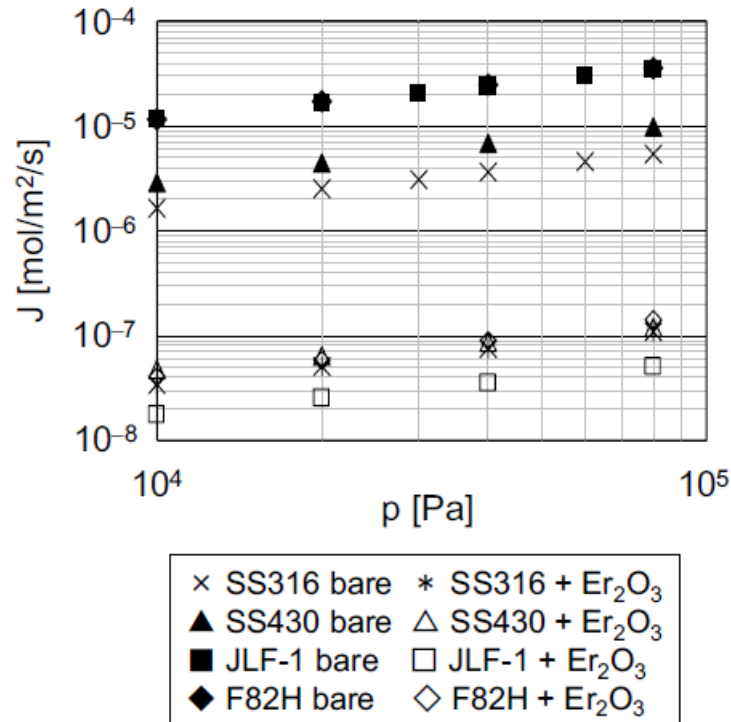


Figure 4.1: Pressure dependence of permeability through bare and  $\text{Er}_2\text{O}_3$  coated samples [45]

The substrate thickness was 0,5 mm, coating compound used was  $\text{Er}_2\text{O}_3$ . Thickness of the coating was roughly 1  $\mu\text{m}$ , slightly depending on deposition time. Coating was deposited either at room temperature or at 973 K. In the latter case, the coating performance was unsatisfactory, coating was peeled off, many lines on the surface appeared and substrate was exposed in some areas. Room temperature deposited coatings did not contain any holes or cracks, the surface was smooth and permeation measurements showed a permeation reduction of 2 to 3 orders of magnitude. Depending on the substrate, the TPRF values differ in range of 1

order. TPRF values of the bare substrate materials differ in the same range. Thus, Chikada et al. made the conclusion that ability of permeation reduction arises from the permeability of substrate [45].

## 4.6 Pack cementation

PC is a two-step technique of aluminization and oxidation. Specimens that are to be coated are immersed in mixture of  $Al_2O_3$  and Al. Then, an activator is added to the mixture and all compounds are heated. During the heating, alumina compounds are formed, they diffuse through the whole pack and deposit on the specimen surface. As a TPB candidate, it was chosen because of its simple facility and procedure required, and high platability. PC can obtain very high values of PRF on regular steel samples, e.g. several  $\mu m$  thick coating on 316L or DIN1.4914 reached PRF of  $10^3 - 10^4$ . However the performance of the barrier on structural components (tubular specimen) was significantly weaker. Hydrogen PRF of aluminide coating inside of 316L steel tube at 623 – 823 K was in the range 30 – 70 [36].

## 4.7 Plasma spraying

The plasma spraying (PS) technique is a procedure when the coating material in the form of powder is introduced in a plasma jet, which melts and propels it onto the substrate. There, the molten droplets flatten and solidify, thereby forming the coating. When fused or half-fused Al powder are sprayed on steel substrate, additional heat-treatment is then required to form aluminide coating. PS can be performed in ambient or inert atmosphere or vacuum and the techniques are distinguished as atmospheric plasma spraying (APS) and vacuum plasma spraying (VPS).

Perujo et al. performed permeation measurements on VPS Al coating on MANET steel and followed by additional heat treatment. Substrate was 0,5 mm thick, coating procedure consisted of pre-heat treatment, austenization, VPS of pure Al – in total 100  $\mu m$  deposited, final heat treatment and oxidation. In total 3 samples were examined, the difference was in temperature and duration of oxidation - 1023 K for 15 hours (1), 1223 K for 10 hours (2), 1223 K for 1 hour (3). Sample 1 and 2 were not deposited successfully, sample 1 did not show any reduction in permeation, sample 2 was in addition extremely brittle and unsuitable for measurements. Sample 3 reached PRF values of about 500 and showed greater crack resistance [46]. Additional heat treatment was applied on samples with 100  $\mu m$  Fe-Al surface layer after deposition. The coating was brittle and contained cracks and delaminations; in spite of this, permeation reduction reached 2-3 orders of magnitude [31]. Experiments with VPS Al on steel substrate showed formation of  $Fe_3Al$  and  $Fe_2Al_5$ , which were well adherent, but contained cracks and delaminations. Despite this, PRF values measured ranged from  $10^2$  to  $10^3$ . After additional post-oxidation,  $Al_2O_3$  layer was formed and PRF values became stable at 500. Further measurements were performed after exposure to Pb-Li, the PRF was reduced due to the formation of  $LiAlO_2$  [22]. Coatings prepared by VPS of Al by Shi et al. were also well adherent to the substrate. The deposition was followed by additional heat treatment and oxidation. The surface contained cracks and delaminations; however, despite of this, the TPRF values ranged 100 – 1000 in air, after oxidation 500. After exposure to Pb-Li, the performance lowered [43].

## Chapter 5

# Remelting of APS $Al_2O_3$ with the use of electron gun – experimental part

### 5.1 Literature survey

Aluminium oxide is one of the most promising materials considered as permeation barrier. As mentioned in section 3, depending on the substrate, technique and physical conditions during the fabrication,  $Al_2O_3$  is capable to lower the permeation rate up to four orders of magnitude. Resulting performance of  $Al_2O_3$  as a permeation barrier depends strongly on its phase composition.  $Al_2O_3$  crystallizes in several phases after deposition, namely  $\alpha$ -,  $\gamma$ - or  $\theta$ - $Al_2O_3$ . It is emphasised not only for vacuum/atmospheric spraying to avoid forming of different phase than  $\alpha$ - $Al_2O_3$ , as this corundum type  $Al_2O_3$  possesses best properties to serve as efficient permeation barrier. This can be assured by several means – adjustment of the deposited matter, changing deposition parameters or by application of suitable post treatment technique. General principle of remelting is to focus heat onto the

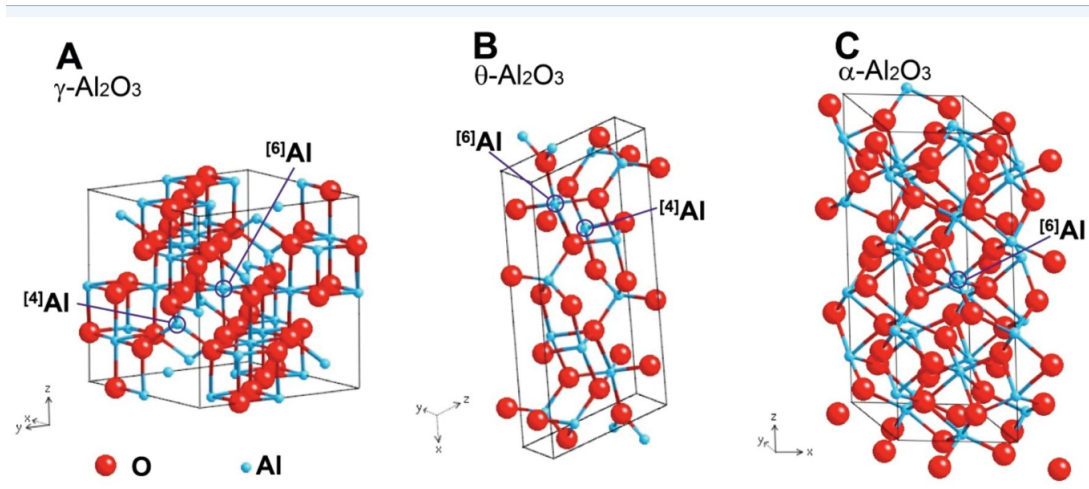


Figure 5.1: Crystallographic phases of Alumina -  $\gamma$ ,  $\theta$  and  $\alpha$  [47]

prepared barrier layer in sufficient amount to melt the layer, but low enough not to harm the substrate material. Then, the layer is let to solidify again, this time in steadier conditions than during the deposition. The resulting layer is supposed to gain different phase structure, if desired, smoother surface without unevenness or defects and improved adhesion to substrate material.

In the experiments published in literature, the most preferred device is laser, although electron gun is also employed in some experiments. Crucial parameters of the method are connected with the laser or electron gun, namely power and diameter of the beam, or in other words power density. Usually larger area of the specimen is treated, so either the source or the specimen is moving in order to provide homogenous remelting of the whole area. This emphasises third vital parameter – velocity of beam/specimen. Quantities describing level of

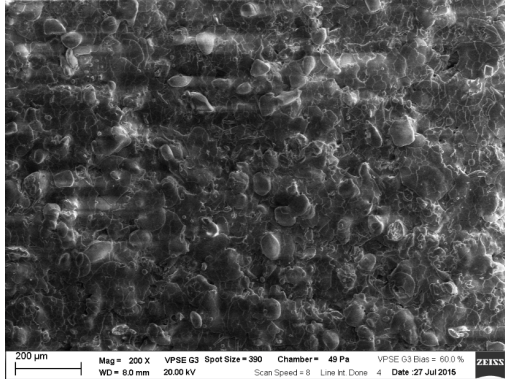


Figure 5.2: As-sprayed surface

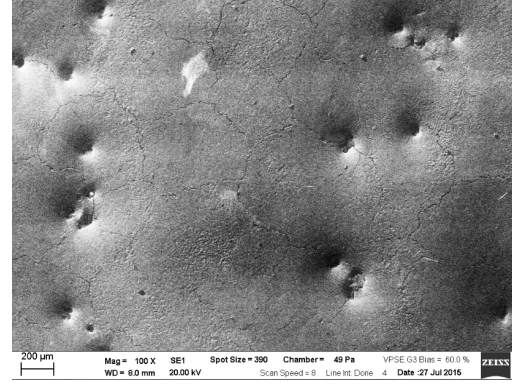


Figure 5.3: Remelted surface

Material type	ST [ $\mu\text{m}$ ]	$RD_{10W}$ [ $\mu\text{m}$ ]	$RD_{30W}$ [ $\mu\text{m}$ ]
Pure $Al_2O_3$	640	122	371
92% $Al_2O_3$	580	71	263
67% $Al_2O_3$	450	71	195
Pure $Cr_2O_3$	510	81	163

Table 5.1: As-sprayed thickness and remelted depths of prepared specimens, ST - As-sprayed thickness,  $RD_{10W}$  - depth of coating remelted with 10 W power,  $RD_{30W}$  - depth of coating remelted with 30 W power [48].

remelting success are mainly remelted depth, phase constitution and surface smoothness. Several measurements conducted on  $Al_2O_3$  have shown that laser is capable to remelt substantial thickness of the layer. Experiments were performed on spraying of the  $Al_2O_3$  and  $Cr_2O_3$  mixture, in order to decrease the amount of  $\gamma - Al_2O_3$  formed in the layer. The sprayed layer was then remelted with  $CO_2$  laser. Four mixtures were prepared, differing in the  $Al_2O_3$  amount – pure  $Al_2O_3$ , 92 % $Al_2O_3$ , 67 % $Al_2O_3$ , pure  $Cr_2O_3$ . Laser power was either 10 W or 30 W, beam diameter was 0,25 mm and velocity was 10 mm/s. Thickness of the deposited layer and remelted thickness when 10 W/30 W was used is in table 5.1. Generally, the lower power resulted in smoother surface, but in lower remelting. Besides, after recrystallizing, waves appeared on the surface along the beam trace. The transition between remelted and not remelted layer was sharp. Remelted part was not porous and it was harder in comparison to pure  $Al_2O_3/Cr_2O_3$ . Remelted material was dense and homogenous in all cases. However, lower heat transfer through the ceramic resulted in crack formation, mostly in the beam direction but also perpendicular to it [48]. The remelted surface is displayed in figures 5.4 to 5.9.

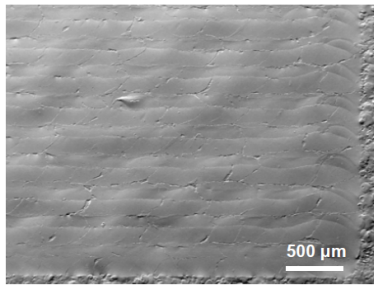


Figure 5.4: Surface of pure alumina coating after 10W laser treatment [48]

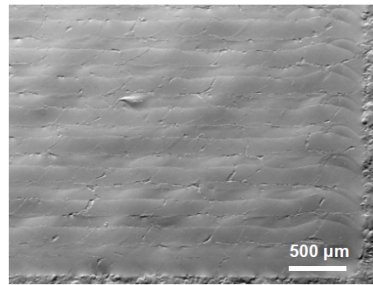


Figure 5.5: Surface of coating containing 67% of alumina after 10W laser treatment [48]

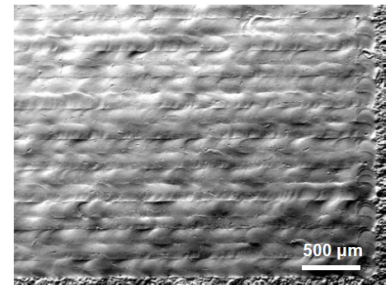


Figure 5.6: Surface of pure chromia coating after 10W laser treatment [48]

Specimen	P [W]	D [cm]	V [cm/s]	$\rho_P$ [kW/cm <sup>2</sup> ]	$\rho_E$ [J/cm <sup>2</sup> ]	RD [ $\mu$ m]
A1	800	0,25	6	16,297	533,3	240
A1	1000	0,25	6	20,372	666,7	263
C1	400	0,2	5	12,732	400	128
C1	500	0,2	5	15,915	500	162
A2	800	0,25	6	16,297	533,3	210
A2	1000	0,25	6	20,372	666,7	-
C2	400	0,2	5	12,732	400	-
C2	500	0,2	5	15,915	500	-
A3	800	0,25	6	16,297	533,3	196
A3	1000	0,25	6	20,372	666,7	223
C3	400	0,2	5	12,732	400	115
C3	500	0,2	5	15,915	500	136
A4	800	0,25	6	16,297	533,3	172
A4	1000	0,25	6	20,372	666,7	210
C4	400	0,2	5	12,732	400	80
C4	500	0,2	5	15,915	500	88
A5	800	0,25	6	16,297	533,3	-
A5	1000	0,25	6	20,372	666,7	209
C5	400	0,2	5	12,732	400	61
C5	500	0,2	5	15,915	500	65

Table 5.2: Parameters of deposited samples, P - power, D - beam diameter, V - beam velocity,  $\rho_P$  - power density,  $\rho_E$  - energy density, RD - remelted depth [49].

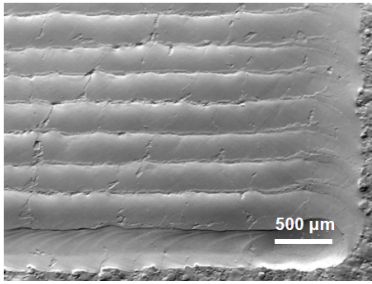


Figure 5.7: Surface of pure alumina coating after 30W laser treatment [48]

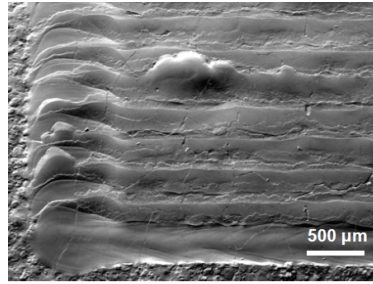


Figure 5.8: Surface of coating containing 67% of alumina after 30W laser treatment [48]

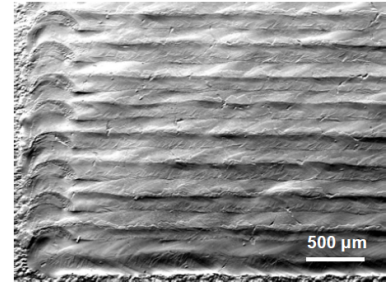


Figure 5.9: Surface of pure chromia coating after 30W laser treatment [48]

Remelting of several types of vacuum sprayed materials was examined by Yuanzheng et al. Compound and composition of sprayed materials is shown in figure 5.10, parameters of samples in table 5.2. Remelting was done with 5 kW  $CO_2$  laser with final power density of 12,7 or 15,9 kW/cm<sup>2</sup> for specimen with compound of  $TiO_2$  and 16,3 or 20,3 kW/cm<sup>2</sup> for specimen without  $TiO_2$ .

Ceramic	Ceramic	Ceramic	Ceramic+3%SiO <sub>2</sub>	Ceramic+8%SiO <sub>2</sub>
Carbon steel	NiCrAl	Ceramic+50%NiCrAl	Ceramic+50%NiCrAl	Ceramic+50%NiCrAl
A1 or C1	Carbon steel	NiCrAl	NiCrAl	NiCrAl
	A2 or C2	Carbon steel	Carbon steel	Carbon steel
		A3 or C3	A4 or C4	A5 or C5

Figure 5.10: Compound and composition of prepared samples [49]

After remelting, A specimen featured thicker remelted layer than C specimen and it was denser than the original material. However, cracks and holes appeared on the surface. The C specimen lost lamellar structure and remelted layer became homogenous, but the thickness was smaller than in the A specimen. It can be concluded that thickness of remelted layer depends on type of composition of sprayed material – specimen that

contained the same elements but differ in percentage of  $SiO_2$  were remelted differently – higher amount of  $SiO_2$  resulted in thinner remelted layer. But providing the same as sprayed layer, the thickness increased with the power density. Not only  $SiO_2$  but also  $TiO_2$  affected the thickness of remelted layer. Apparently the lamellar structure and lower thermal conductivity implies that  $TiO_2$  acts as a thermal barrier [49]. Ctibor et al. conducted experiments of laser remelting of  $Al_2O_3$  and  $Zr_2O_3$  PS specimens. Laser power was 2 kW, wavelength 1,06  $\mu m$ , beam diameter 10 mm. Steel was used as a substrate and two types of material were used:  $Zr_2O_3$  with 7,9 % $Y_2O_3$  (named YSZ) and  $Al_2O_3$  with 4,7 % $TiO_2$  and 1,4 % $Fe_2O_3$  (AG). Energy density and laser velocity

Sample label	Energy density $E$ (J/mm <sup>2</sup> )	Laser scanning velocity $v$ (mm/min)	Plasma spray distance $SD$ (mm)
YSZ	-	-	300
YSZ 5	5	2400	300
YSZ 15	15	800	300
YSZ 20	20	600	300
YSZ 25	25	475	300
YSZ 30	30	400	300
AG 300	-	-	300
AG 300 6	6	2000	300
AG 400 6	6	2000	400
AG 300 7	7	1700	300
AG 400 7	7	1700	400
AG 400 8	8	1500	400

Figure 5.11: Deposition and post-treatment parameters of examined samples [50]

were set precisely, so that the product was constant. That implied energy density 5 – 30 J/mm<sup>2</sup> and velocity 400 – 2400 mm/min for YSZ specimen and 6-8 J/mm<sup>2</sup> and 1500 – 2000 mm/min for AG specimen, as seen in figure 5.11. Overall results have shown that both remelting of  $Al_2O_3$  and  $Zr_2O_3$  was successful and decreased porosity, although in case of  $Zr_2O_3$ , surface integrity was slightly worse. Higher effect on the material was seen when higher energy density and smaller beam velocity was used. YSZ specimen possessed smooth surface after remelting, the layer was dense and the thickness was up to 300  $\mu m$ . Surface of AG specimen was rougher and contained more defects and pores than YSZ, also the remelted layer was thinner; the best results showed thickness of about 100  $\mu m$ . Also experiments of remelting  $Al_2O_3$  with 4 % addition of  $TiO_2$  were conducted. 2 kW laser with beam diameter 10 mm was used and in total 3 combinations of energy density and beam velocity were set: 6 J/mm<sup>2</sup> – 2000 mm/min, respectively 7 – 1700 and 8 – 1500. First specimen has shown almost no remelting, only about 200  $\mu m$  were affected by laser, the surface was damaged by cracks and overall has shown poor results. At middle setting 50  $\mu m$  of layer were remelted and another 300 – 350  $\mu m$  were affected. Lastly, 80  $\mu m$  were remelted and 200  $\mu m$  affected [50].

## 5.2 Remelting experiments and results

The performed experiments were focused on change of structure and surface properties of plasma sprayed  $Al_2O_3$ . Remelting with electron beam was chosen as post treatment technique. The specimens were prepared in the Institute of Plasma Physics CAS in Prague by Jiří Matějčík. WSP-H torch with argon-water stabilization, using Surprex AW24 powder (Fujimi, Japan) with a 63-100  $\mu m$  size range. Feeding distance was 65 mm, spraying distance was 360 mm, feed rate was 10 kg/h. 2,5 mm thick low carbon steel was used for substrates, these were preheated to 100 °C. In total three series were prepared, varying in thickness of the  $Al_2O_3$  layer – approximately 100  $\mu m$ , 200  $\mu m$  and 300  $\mu m$ . Remelting was performed at VUT in Brno under supervision of Ing. Jan Čížek and Bc. Jan Kouřil on the NETME facility. The biggest advantage of the facility is its ability to adjust the power of the beam and the size of treated area. Therefore it is possible to remelt, weld or cut the material just by changing the beam power.

The aim of our experiments was to remelt complete  $Al_2O_3$  layer and to obtain smooth surface without any imperfections. As only limited number of specimens was available, reasonable parameters to get in touch with the facility were chosen for the first attempts and before another series of remelting, the characteristics of the previously remelted specimen were examined. The examination consisted of metallographical treatment that revealed the cross section of the specimen. The cross section and surface of the specimen were observed using the optical microscope and on behalf of these observations the parameters for the next set of experiments were determined. Later observations in Prague were performed with scanning electron microscope, in order to gain more detailed information about the structure. It was decided that until promising results are achieved, all experiments would be performed on 100  $\mu m$  samples. It has taken 6 series, before the observations from optical microscope indicated promising surface and cross section features. After this breakthrough, the most promising series were repeated on thicker specimen and following parameters were applied on all three types of specimens. This approach resulted in 33 remelted specimens, from which 24 were identified as the most promising and were examined using the SEM.

Parameters used in the remelting of all specimens are shown in table 5.3. Voltage of 120 kV and beam diameter of 20 mm were used in all cases. Voltage and current determine the total power of the beam, diameter and velocity determine the power density of the beam. The abbreviations reflects the series of experiment – 1 to 10, type of specimen used, according to the sprayed layer thickness – 1 for 100  $\mu m$ , 2 for 200 and 3 for 300, and number of treatments (beam passes) – A for 1, B for 2, except for series 5. As mentioned above, series 1 to 5 were just preliminary, the main objective was to acquire confirmation that any surface/structure changes occur after treatment with electron gun and to get familiar with possibilities of the machine. First remelted specimen; 1,2 and 3; proved the applicability of electron gun and established the background for other series.

During the treatment was found that the whole process is rather time demanding, therefore the specimen were divided in half and double sets of parameters were examined simultaneously since. After examination using the optical microscope, decision was made, based on experience of Ing. Čížek, that better results might be achieved by selecting lower current and higher beam velocity. Before adjusting the parameters, specimen 4A/4B were remelted in order to test the effect of multiple treatment, particularly double remelting with identical parameters. Specimen 5A/5B were already remelted using the experience of Ing. Čížek. Results of series 5 were not entirely persuasive, on the other hand, double treatment showed possible improvement of surface performance. It was decided that for all following series, one half of specimen will be treated once, whereas the other half will be double treated. Because of the unclear results of specimen 5A/5B, series 6 and 7 were remelted with distinct difference in beam velocity, in order to finally clarify the most suitable option. Whereas series 6 (beam velocity 20 mm/s) was successful, series 7 (beam velocity 2 mm/s) was considered as non-perspective and final series 8,9 and 10 were based on these results and in these series, all three specimen types were used.

Series 10 is an exception, because of the shortage of 100  $\mu m$  substrate specimen, remelting was conducted only using specimen types 2 and 3. In addition, specimen types 2 and 3 were remelted using parameters from series 6 for comparison. Series 1 to 7 were originally examined using optical microscope in Brno, not to gain exact figures about remelted depth, only to find out overall properties of surface and cross section. Precise measurements on SEM were done only on series 6,8,9 and 10. Specimens 62A/B possessed smooth surface with only sporadic imperfections after remelting, differences between A and B were negligible. Measurements of cross section showed greater difference: the boundary between remelted and unaffected zone was smoother in case

Specimen	Specimen type	I [mA]	V [mm/s]	Double treatment [+/-]
1	1	10	5	-
2	1	8	5	-
3	1	12	5	-
4A	1	6	5	-
4B	1	6	5	+
5A	1	8	7	-
5B	1	8	9	-
6A	1	6	20	-
6B	1	6	20	+
7A	1	6	2	-
7B	1	6	2	+
62A	2	6	20	-
62B	2	6	20	+
63A	3	6	20	-
63B	3	6	20	+
8A	1	6	40	-
8B	1	6	40	+
82A	2	6	40	-
82B	2	6	40	+
83A	3	6	40	-
83B	3	6	40	+
9A	1	3	20	-
9B	1	3	20	+
92A	2	3	20	-
92B	2	3	20	+
93A	3	3	20	-
93B	3	3	20	+
102A	2	9	20	-
102B	2	9	20	+
103A	3	9	20	-
103B	3	9	20	+

Table 5.3: Parameters of remelting, I - remelting current, V - beam velocity

of A specimen. However, the thickness was similar: 50 to 70  $\mu m$ . Results of specimen 63A and B were worse than in the previous specimen. 63A possessed minor inhomogeneities in composition and small depressions in the surface. Thickness of the remelted layer was 60 to 80  $\mu m$ . Remelting of 63B was successful on the whole surface, but noticeable cracks occurred. Remelted thickness was similar to 63A – 60 to 80  $\mu m$ . The surface photos can be seen in figures 5.12 and 5.13, the cross sections in figures 5.14 and 5.15.

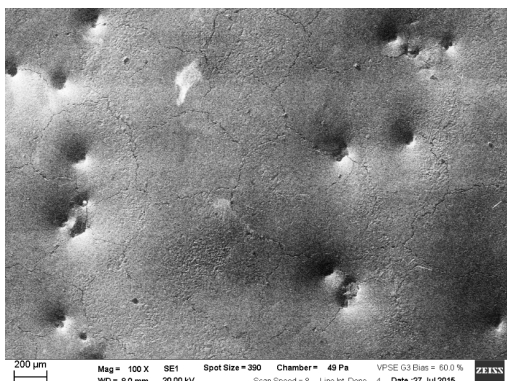


Figure 5.12: Sample 63A - surface

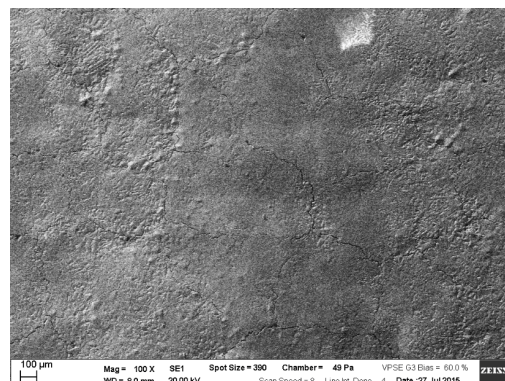


Figure 5.13: Sample 63B - surface

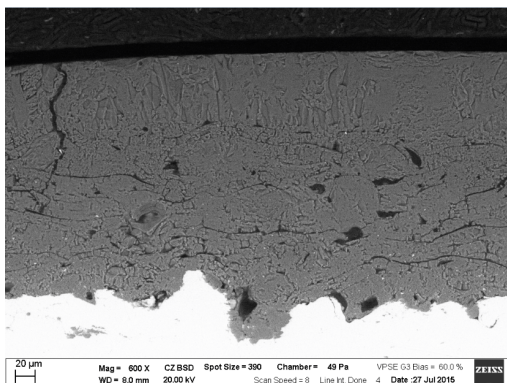


Figure 5.14: Sample 63A - cross section

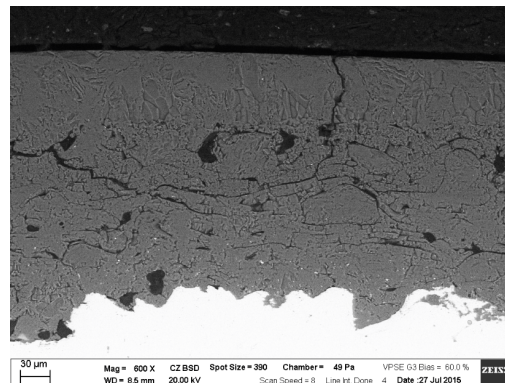


Figure 5.15: Sample 63B - cross section

Surface results of specimen from series 8 worsen with increasing substrate layer thickness. Thickness of the remelted layer slightly increased, but did not exceed 40  $\mu m$ . Surface of specimen 8A was smooth only at less than half the area and the remelting damaged the surface significantly (5.16). Areas with successful remelting occurred very rarely and the thickness was approximately 20  $\mu m$  (5.18). Surface of 8B was smooth on approximately half, on the other half was rather rough (5.17). The boundary at the cross section was very wavy and also only few successfully remelted areas were detected. 82A/B were remelted almost smoothly, although small and shallow depressions were very frequent. Cross section of 82A showed almost continuous remelted layer with thickness of 20 to 40  $\mu m$  (5.19). 82B possessed more wavy and cracked boundary than A, with slightly thinner layer.

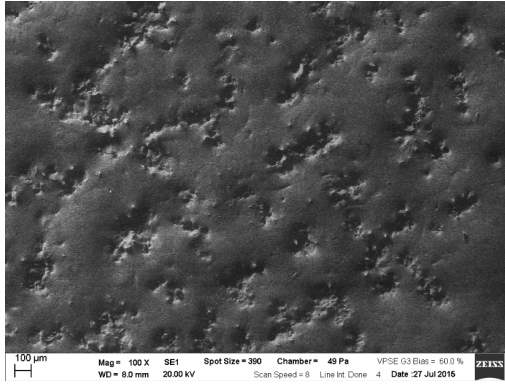


Figure 5.16: Sample 82A - surface

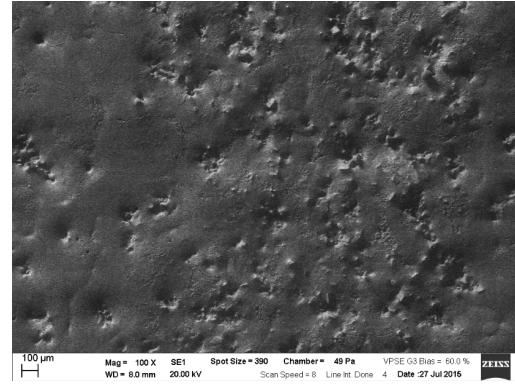


Figure 5.17: Sample 82B - surface

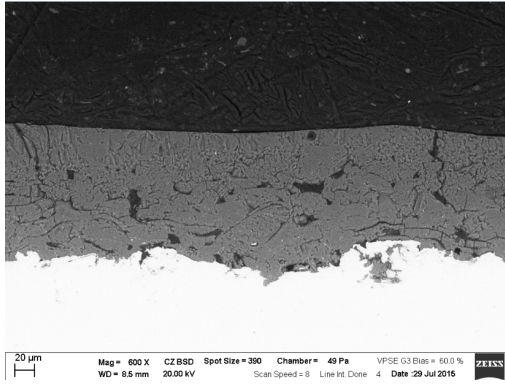


Figure 5.18: Sample 82A - cross section

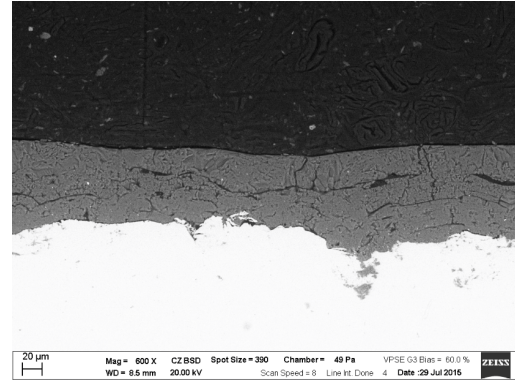


Figure 5.19: Sample 82B - cross section

Surface of 83A was very diverse, in the middle there were more depressions and some holes in the layer occurred, on the edges, the surface was more continuous (5.20). Thickness of the remelted layer was 20 to 30  $\mu m$ , with rare exceptions up to 50  $\mu m$ (5.22). 83B contained depressions very often, the density was uneven and remelted depth reached only about 30  $\mu m$ . Surface photo is in figure (5.21) and cross section (5.23).

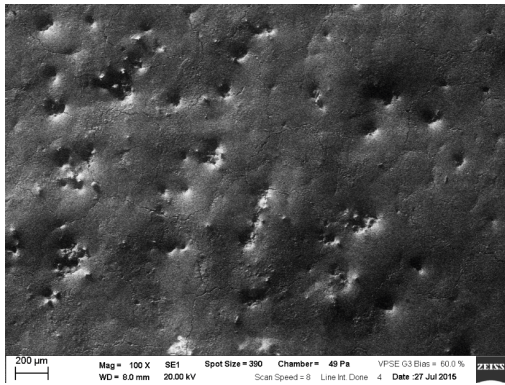


Figure 5.20: Sample 83A - surface

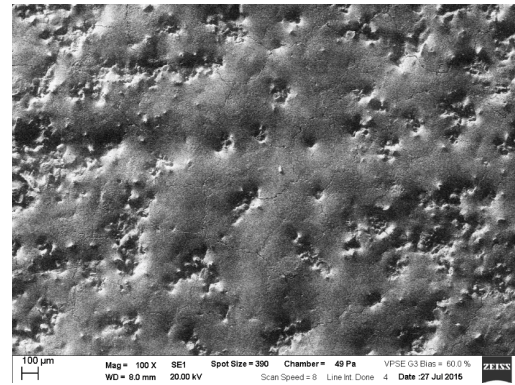


Figure 5.21: Sample 83B - surface

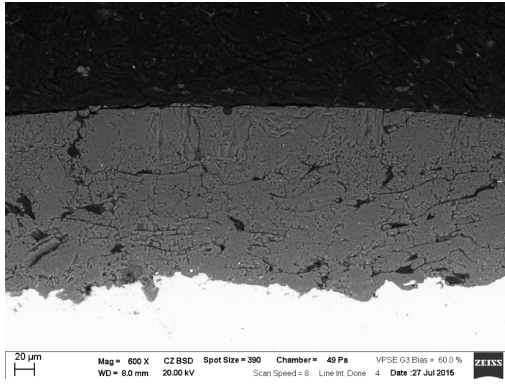


Figure 5.22: Sample 83A - cross section

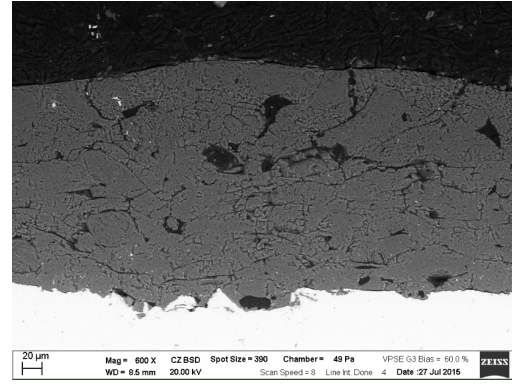


Figure 5.23: Sample 83B - cross section

Specimen 9A/B showed almost unaffected surface and cross section (5.24, 5.25, 5.26, 5.27). Remelted areas at 9A were negligible, very few were found on the cross section of 9B with thickness 20 to 40  $\mu\text{m}$ .

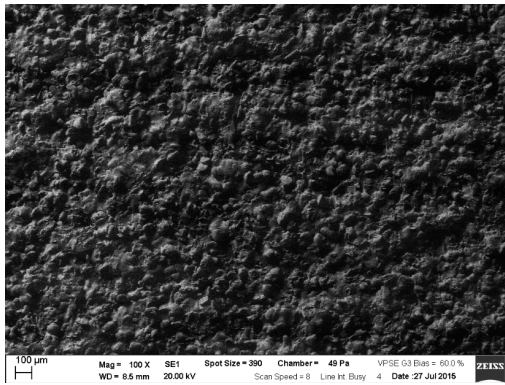


Figure 5.24: Sample 9A - surface

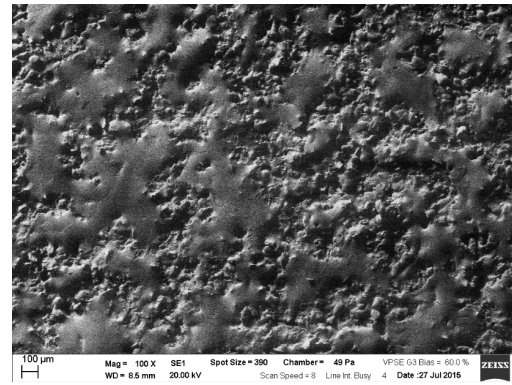


Figure 5.25: Sample 9B - surface

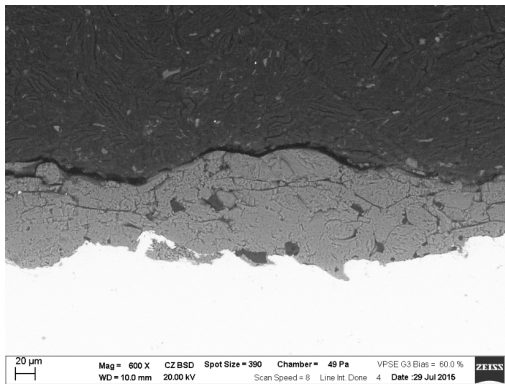


Figure 5.26: Sample 9A - cross section

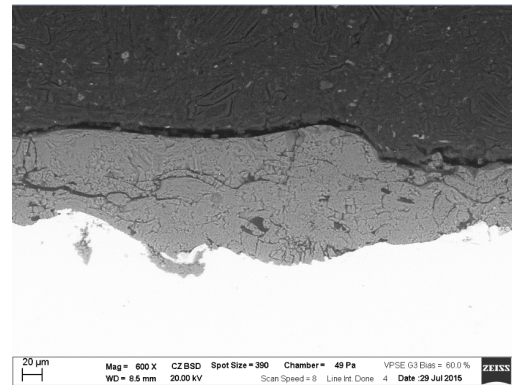


Figure 5.27: Sample 9B - cross section

Performance of 92A/B was slightly better, but neither those specimens showed significant remelted area (5.28). 92A showed more than half the surface as smooth, however the cross section revealed non-continuous layer, significantly peeled off. Very few remelted areas were identified with thickness 20 to 35  $\mu\text{m}$ . Surface on 92B was unevenly remelted too, ratio of smooth:rough approximately 1:1. The cross section was very similar to 92A, non-continuous, peeled off and very few remelted areas, 10 to 30  $\mu\text{m}$  (5.29).

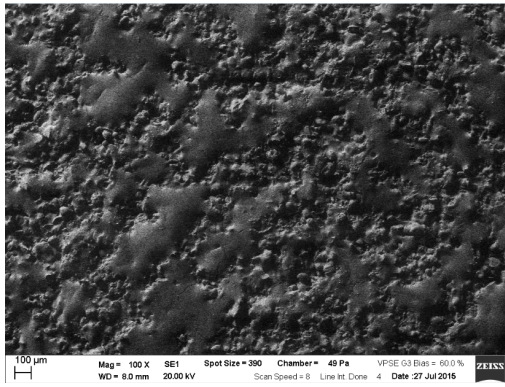


Figure 5.28: Sample 92B - surface

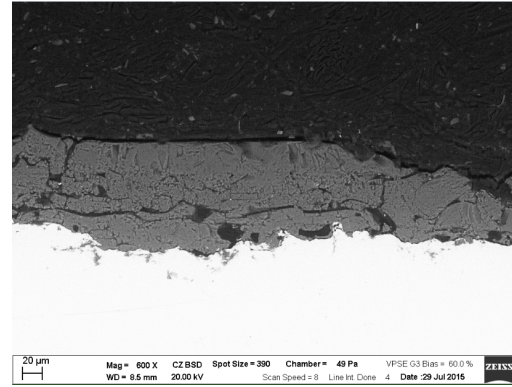


Figure 5.29: Sample 92B - cross section

Surface of 93A was only slightly affected, morphology of as-sprayed layer was partly concealed. Cross section measurements showed remelted depth around  $30 \mu\text{m}$ . Specimen 93B possessed similar quality, surface was almost continuously remelted, although depressions occurred often. Remelted depth was very similar too, about  $30 \mu\text{m}$ . Surface of 102A contained only few depressions, but rough areas were larger. The remelted layer was almost continuous, only few depressions were present. Very rarely, they reached up to the boundary, but thickness of the layer exceeded  $100 \mu\text{m}$  frequently,  $100$  to  $150 \mu\text{m}$ . Specimen 102B contained more depressions, some of them reached even the bare substrate steel(5.30). The cross section was slightly wavy and on the rare occasions, cracks and thinner areas occur, overall the layer was smooth and continuous. Thickness was slightly smaller than at 102A,  $70$  to  $100 \mu\text{m}$ (5.31).

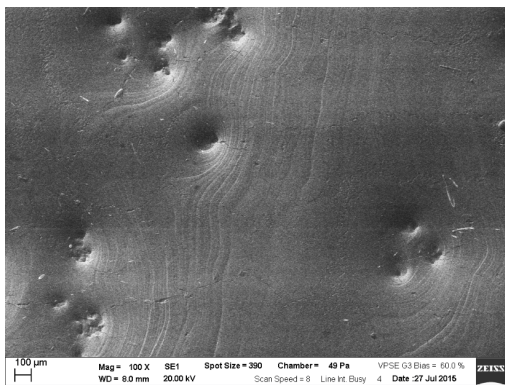


Figure 5.30: Sample 102B - surface

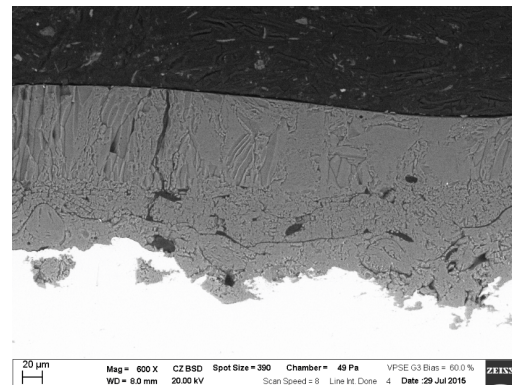


Figure 5.31: Sample 102B - cross section

Specimen 103A/B possessed the greatest thickness of remelted layer out of all examined specimens. Surface of 103A was continuous, very few depressions occurred, but none of them reached the steel substrate, at the bottom of all depressions there was remelted  $\text{Al}_2\text{O}_3$ (5.32). Cross section was slightly wavy, more than later at 103B, in the thinner areas, thickness varied between  $70$  to  $100 \mu\text{m}$ , and in the thicker areas reached almost  $150 \mu\text{m}$ (5.34). Surface of 103B was continuous too, few cracks occurred, but very distant in comparison with earlier specimen(5.33). The cross section was smooth and straight, at very few occasions horizontal cracks occurred, but solely in the transition area between 103A and 103B. The thickness of remelted layer was balanced:  $120$  to  $150 \mu\text{m}$ (5.35).

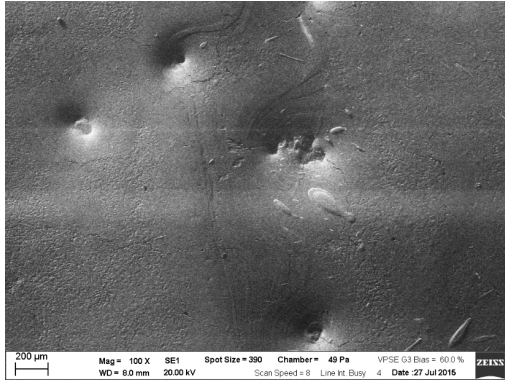


Figure 5.32: Sample 103A - surface

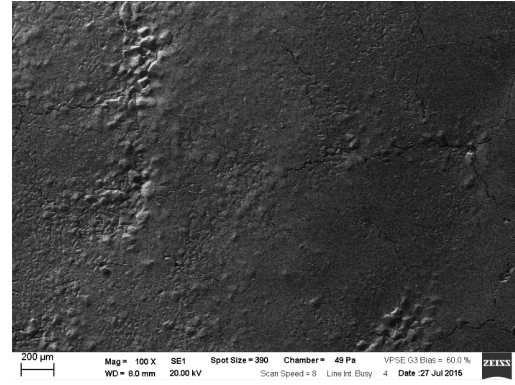


Figure 5.33: Sample 103B - surface

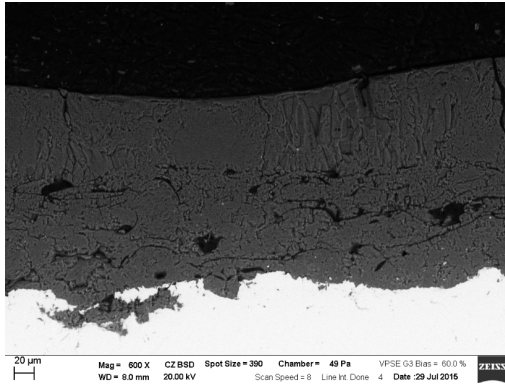


Figure 5.34: Sample 103A - cross section

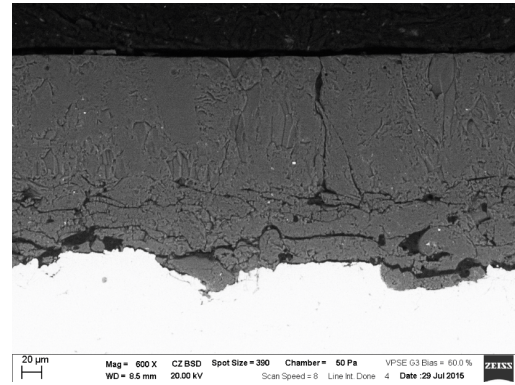


Figure 5.35: Sample 103B - cross section

Remelting of the samples was expected to affect not only surface roughness, but also its hardness and phase constitution. For the hardness testing, samples 63B, 83B, 93B and 103B were selected. Testing was performed with Vickers indenter and 100g weight for 10 seconds. Measured values of hardness are in table 5.4. Average values are  $(804 \pm 69)$  HV/  $(2491 \pm 52)$  HV for 63B as-sprayed/remelted,  $(761 \pm 62)$  HV/  $(2468 \pm 146)$  HV for 83B as-sprayed/remelted,  $(1190 \pm 41)$  HV/  $(2459 \pm 88)$  HV for 93B as-sprayed/remelted and  $(719 \pm 71)$  HV/  $(1910 \pm 78)$  HV for 103B as-sprayed/remelted. Hardness of the remelted specimens is 2-3 times greater than of the as-sprayed, as seen in table 5.4. It implies that cracks and pores were sealed by the remelting. X-ray diffraction results showed that the as-sprayed coatings contained 86 % of  $\gamma$  alumina and 14 %  $\alpha$ -alumina.  $\gamma$ -alumina is a metastable phase whose formation results from the rapid solidification during plasma spraying. The remelted layer in samples 103B and 63B consists of only  $\alpha$ -alumina, indicating much slower solidification after the remelting. Results from the diffraction are shown in figures 5.36 and 5.37.

63B as	63B rem	83B as	83B rem	93B as	93B rem	103B as	103B rem
656	2021	1097	1979	1290	2405	484	1821
841	2490	586	2268	1103	2237	851	2413
784	2399	645	2788	1151	2632	807	2171
1074	2602	714	2779	1217	2563	522	1709
686	2754	809	2967			472	2064
548	2372	731	2063			459	1751
1101	2632	748	2433			441	2243
744	2281					532	1619
	2556					1293	1939
	2805					1063	1387
						490	1713
						488	1282
						1274	1764
						1064	1990
						721	2032
						720	2294
						542	2483
							1705
804 ± 69	2491 ± 52	761 ± 62	2468 ± 146	1190 ± 41	2459 ± 88	719 ± 71	1910 ± 78

Table 5.4: Hardness of as-sprayed (as) and remelted (rem) samples, average values are written in the last line

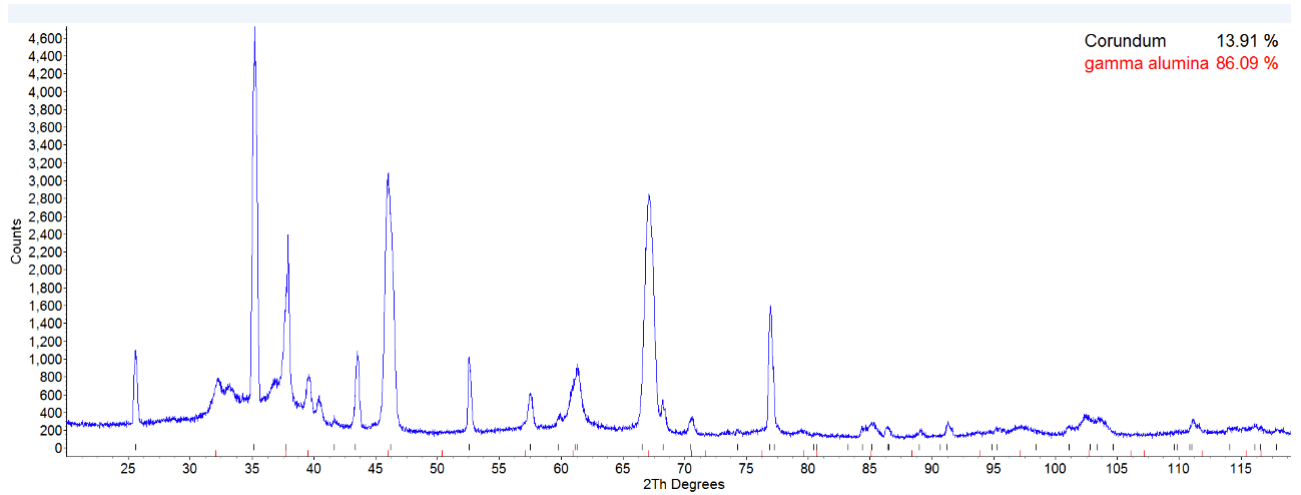


Figure 5.36: Results of X-ray diffraction from as-sprayed samples

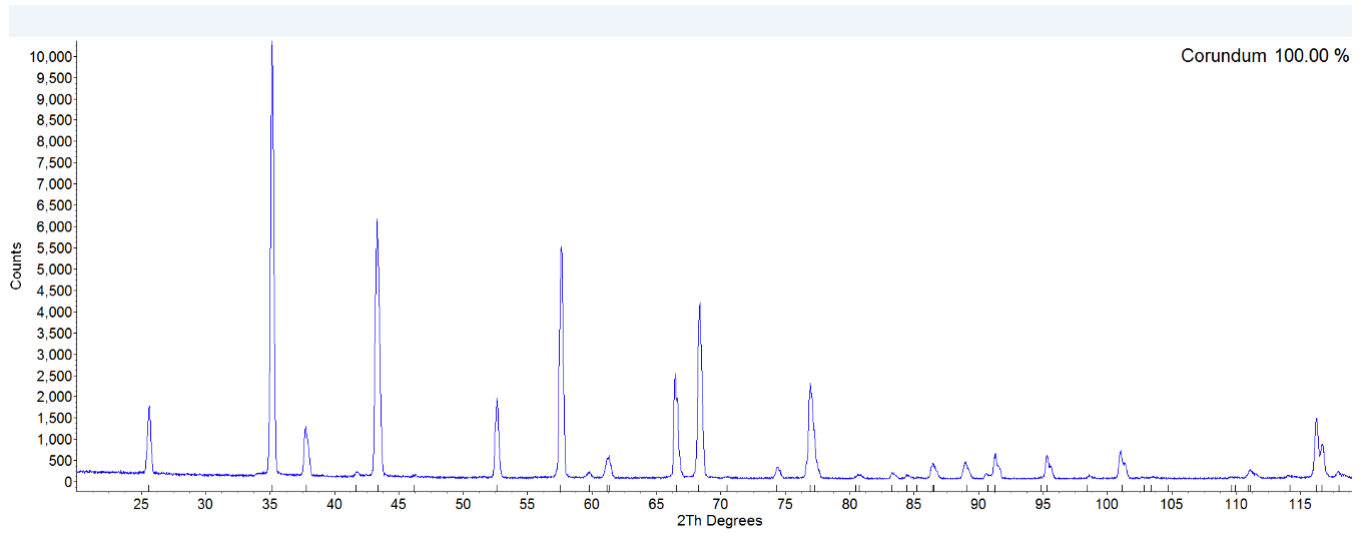


Figure 5.37: Results of X-ray diffraction from remelted sample 103B

## Chapter 6

# Summary

In total 7 designs of TBM are discussed for ITER. Individual designs differ in numerous aspects, e.g.: internal structure, type of breeder, type of coolant etc. Choice of the breeder influences the role of the barriers: In designs with liquid Pb-Li, permeation barriers act additionally as corrosion barriers. Literature survey showed that the most promising materials are oxidic ceramics ( $Al_2O_3$ ,  $Cr_2O_3$ ..), along with thin layers of nitrides or carbides. There are several potential deposition techniques - physical vapor deposition, hot-dip aluminization, electrochemical deposition or plasma spraying. Experiments confirmed that remelting with electron beam is capable of producing smooth  $Al_2O_3$  surface layer with more than 100  $\mu m$  thickness. XRD confirmed the change of composition from  $\gamma - Al_2O_3$  to  $\alpha - Al_2O_3$  and hardness measurements showed that after remelting, the hardness increased 2-3 times. Experiments therefore confirmed that the production of potential permeation barrier with plasma spraying, followed by remelting, is possible. Next step would be measuring of permeation through bare and coated sample and identifying, if the performance would be sufficient. That is currently discussed with facility in Jülich, Germany.

# Bibliography

- [1] Meier W.R. Assessment of tritium breeding blankets from a systems perspective - status report. Lawrence Livermore National Laboratory, 2014.
- [2] Demange D.; Boccaccini L.V.; Franza F.; Santucci A.; Tosti S.; Wagner R. Tritium management and anti-permeation strategies for three different breeding blanket options foreseen for the European powerplant physics and technology demonstration reactor study. 2014.
- [3] Raffray A.R.; Akiba M.; Chuyanov V.; Giancarli L.; Malang S. Breeding blanket concepts for fusion and materials requirements. Journal of Nuclear Materials, 2002.
- [4] Cheng X.; Ma X.; Jiang K.; Chen L.; Huang K.; Liu S. Thermal hydraulic design and analysis of a water-cooled ceramic breeder blanket with superheated steam for CFETR. Plasma Science and Technology, 2015.
- [5] Giancarli L.M.; Abdou M.; Campbell D.J.; Chuyanov V.A.; Ahn M.Y.; Enoda M.; Pan C.; Poitevin Y.; Rajendra Kumar E.; Ricapito I.; Strebkov Y.; Suzuki S.; Wong P.C.; Zmitko M. Overview of the ITER TBM program. Fusion Engineering and Design 87, 395-402, 2012.
- [6] Krauss W.; Konys J.; Holstein N.; Zimmermann H. Al-based anti-corrosion and t-permeation barrier development for future demo blankets. Journal of Nuclear Materials, 2011.
- [7] Gastaldi O.; Ghirelli N.; Gabriel F. Giancarli L.; Salavy J.F. Tritium transfers and main operating parameters impact for demo lithium lead breeding blanket (HCLL). Fusion Engineering and Design, 2008.
- [8] Ehrlich K.; Gasparotto M.; Giancarli L.; Le Marois G.; Malang S.; van der Schaff B. European material assessment meeting. 2001.
- [9] Causey R.A.; Karnesky R.A.; San Marchi Ch. Tritium barriers and tritium diffusion in fusion reactors. Sandia National Laboratories, 2009.
- [10] Hollenberg GW; Simonen EP; Kalinin G; et al. Tritium hydrogen barrier development. Fusion Engineering and Design, 1995.
- [11] Levchuk D; Koch F; Maier H. Deuterium permeation through EUROFER and alpha-alumina coated EUROFER. Journal of Nuclear Materials, 2004.
- [12] Forcey KS; Ross DK; Simpson JCB. The use of aluminizing on 316L austenitic and 1.4914 martensitic steels for the reduction of tritium leakage from the net blanket. Journal of Nuclear Materials, 1989.
- [13] Forcey KS; Ross DK and Wu Ch. The formation of hydrogen permeation barriers on steels by aluminizing. Journal of Nuclear Materials, 1991.
- [14] Forcey KS; Perujo A; Reiter F; et al. Analysis of the hydrogen permeation properties of tin-titanium bilayers deposited on martensitic stainless steel. Surface and Coatings Technology, 1996.
- [15] Forcey KS; Ross DK; Simpson JCB. The formation of tritium permeation barriers by CVD. Journal of Nuclear Materials, 1993.
- [16] Coen V; et al. Conrad R; Debarberis ;. Irradiation of liquid breeder material Pb-17Li with in situ tritium release measurements in the LIBRETTO 2 experiment. Journal of Nuclear Materials, 1991.

- [17] Conrad R; Futterer MA; Giancarli L; et al. Libretto-3 - performance of tritium permeation barriers under irradiation at the hfr petten. Journal of Nuclear Materials, 1994.
- [18] Magielsen AJ; Bakker K; Chabrol C; et al. In-pile performance of a double-walled tube and a tritium permeation barrier. Journal of Nuclear Materials, 2002.
- [19] Proust E; Leroy P and Franenberg HW. Preliminary interpretation of the libretto-2 experimental results in terms of tritium permeation barrier efficiency. Journal of Nuclear Materials, 1992.
- [20] Sherman S.R.; Adams M.T. Tritium barrier materials and separation systems for the ngnp. Savannah River National Laboratory, 2008.
- [21] Hydrogen permeation through the material. [online], <http://www.sigma-tech.it/00immagine/foto/pdimage.jpg>, 6 January 2016.
- [22] Matejicek J.; Chraska P. Development of advanced coatings for iter and future fusion devices. Advances in Science and Technology, vol. 66 (2010) pp 47-65.
- [23] Smith D.L.; Park J.H.; Lyublinski I.; Evtikhin V.; Perujo A.; Glassbrenner H.; Terai T.; Zinkle S. Progress in coating development for fusion systems. Fusion Engineering and Design, 2002.
- [24] Hatano Y.; Zhang K.; Hashizume K. Fabrication of zro2 coatings on ferritic steel by wet-chemical methods as a tritium permeation barrier. Technical report, Hydrogen Isotope Research Center, University of Toyama, 2011.
- [25] He D.; Li S.; Liu X.; Zhang Ch.; Yu O.; Wang S.; Jiang L. Preparation of cr2o3 film by mocvd as hydrogen permeation barrier. Fusion Engineering and Design, 2014.
- [26] Hecker R; Stöver D; Jonas H; et al. Properties of chromia scales on hightemperature alloys used as barriers against hydrogen permeation. Journal of Nuclear Materials, 1990.
- [27] Nakamichi M; Nakamura H; Hayashi K; et al. Impact of ceramic coating deposition on the tritium permeation in the japanese iter-tbm. Journal of Nuclear Materials, 2009.
- [28] Maa W.; Chikada T.; Shimura K.; Suzuki A.; Teraia T. Energetics and diffusion of hydrogen in  $\alpha - al_2o_3$  and  $er_2o_3$ . Fusion Engineering and Design, 2013.
- [29] Hollenberg G.W.; Simonen E.P.; Kalinin G.; Terlain A. Tritium/hydrogen barrier development. Fusion Engineering and Design, 1995.
- [30] Koch F.; Brill R.; Maier H.; Levchuk D.; Suzuki A.; Muroga T.; Bolt H. Crystallization behavior of arc-deposited .ceramic barrier coatings. Journal of Nuclear Materials 329 (2004) 1403-1406.
- [31] Perujo A.; Sample T.; Serra E. and Kolbe H. Low aluminium content permeation barrier coatings for din 1.4914 martensitic steel (manet). FUSION TECHNOLOGY of Nuclear Materials, 1995.
- [32] Chikada T.; Suzuki A.; Adelhelm C.; Terai T. and Muroga T. Surface behaviour in deuterium permeation through erbium oxide coatings. [online], published 13 May 2011.
- [33] Chikada T.; Suzuki A.; Tanaka T.; Teraia T.; Muroga T. Microstructure control and deuterium permeability of erbium oxide coating on ferritic/martensitic steels by metal-organic decomposition. Fusion Engineering and Design, 2010.
- [34] Levchuk D.; Levchuk S.; Maier H.; Bolt H.; Suzuki A. Erbium oxide as a new promising tritium permeation barrier. Journal of Nuclear Materials, 2007.
- [35] Chikada T.; Suzuki A.; Tanaka T.; Naitoh S.; Teruya T.; Muroga T. Deuterium permeation through erbium oxide coatings on rafin steels by a dip-coating technique. Journal of Nuclear Materials, 2013.
- [36] Xin X.; Wang X.; Zhang G.; Tang T.; Lai X. Preparation technique and alloying effect of aluminide coatings as tritium permeation barriers: A review. China Academy of Engineering Physics, 2015.
- [37] Benamati G.; Chabrol C.; Perujo A.; Rigal E.; Glasbrenner H. Development of tritium permeation barriers on al base in europe. Journal of Nuclear Materials, 1999.

- [38] Aiello A.; Ciampichetti A.; Benamati G. An overview on tritium permeation barrier development for well blanket concept. Journal of Nuclear Materials, 2004.
- [39] Forcey K.S.; Perujo A. Tritium permeation barriers for fusion technology. Fusion Engineering and Design, 1995.
- [40] Forcey K.S.; Perujo A.; Reiter F. and Lolli-Ceroni P.L. The formation of tritium permeation barriers by cvd. Journal of Nuclear Materials, 1993.
- [41] Natali M.; Carta G.; Rigato V.; Rossetto G.; Salmaso G.; Zanella P. Chemical, morphological and nano-mechanical characterization of  $al_2o_3$  thin films deposited by metal organic chemical vapors deposition on aisi 304 stainless steels. Electrochim Acta 2005;50:4615-20, 2005.
- [42] Nakamichi M.; Kawamura H.; Teratani T.(2001). Characterization of chemical densified coatings as tritium permeation barrier. journal of Nuclear science and technology, 38:11, 1007-1013, DOI: 10.1080/18811248.2001.9715130.
- [43] Shi Z.; Cao J.; Han F. Preparation and characterization of fe-al intermetallic layer on the surface of t91 heat-resistant steel. Journal of Nuclear Materials, 2014.
- [44] Glasbrenner H.; Perujo A.; Serra E. Hydrogen permeation behaviour of hot-dip aluminized manet steel. FUSION TECHNOLOGY, 1995.
- [45] Chikada T.; Suzuki A.; Levchuk D.; Kobayashi T.; Yao Z.; Maier H.; Takayuki T.; Muroga T. Thermal influence on erbium oxide coating for tritium permeation barrier. FUSION SCIENCE AND TECHNOLOGY, 2009.
- [46] Perujo A.; Serra E. Hydrogen permeation rate reduction by post-oxidation of aluminide coatings on din 1.4914 martensitic steel (manet). Journal of Nuclear Materials, 1996.
- [47] Crystallographic phases of alumina. [online], <http://ammin.geoscienceworld.org/content/98/7/1198/F1.large.jpg>, 13 February 2016.
- [48] Dubsky J.; Kolman B.; Chraska P.; Jancarek A. Laser post-treatment of plasma sprayed  $al_2o_3-cr_2o_3$  coatings. Proceedings of the 2006 International Thermal spray Conference, 2006.
- [49] Yuanzheng Y.; Youlan Z.; Zhengyi L.; Yuzhi Ch. Laser remelting of plasma sprayed  $al_2o_3$  ceramic coatings and subsequent wear resistance. Material Science and Engineering A291, 168-172, 2000.
- [50] Ctibor P.; Kraus L.; Tuominen J.; Vuoristo P; Chraska P. Improvement of mechanical properties of alumina and zirconia plasma sprayed coatings induced by laser post-treatment. Ceramics 51 (4), 181-189, 2007.